UNIVERSITÉ DU QUÉBEC À RIMOUSKI

Interactions vagues-glace dans l'estuaire et le golfe du Saint-Laurent

Mémoire présenté

dans le cadre du programme de maîtrise en océanographie

en vue de l'obtention du grade de maître ès sciences

PAR

© ELIOTT BISMUTH

Septembre 2014

Composition du jury :

Cédric Chavanne, président du jury, UQAR-ISMER

Urs Neumeier, directeur de recherche, UQAR-ISMER

Dany Dumont, codirecteur de recherche, UQAR-ISMER

Natacha Bernier, examinatrice externe, Environnement Canada

Dépôt initial le 19 septembre 2014 Dépôt final le 13 février 2015

Ce que nous accomplissons n'est qu'une goutte dans l'océan. Mais si cette goutte n'existait pas dans l'océan, elle manquerait.

Mère Teresa

REMERCIEMENTS

Je tiens tout d'abord à remercier mon directeur, Urs Neumeier, pour la confiance qu'il m'a accordée en m'offrant ce projet de maîtrise. C'est grâce à sa rigueur scientifique que j'ai pu mener ce projet de maîtrise à terme, et je lui en suis très reconnaissant. Je le remercie aussi beaucoup de m'avoir donné la chance d'embarquer à bord du Coriolis II à quatre reprises pour des missions scientifiques, ainsi que pour les trois congrès scientifiques auxquels j'ai participé.

Je souhaite également remercier mon co-directeur, Dany Dumont, dont la curiosité scientifique, l'enthousiasme et l'intérêt pour mon travail m'a été d'une précieuse aide dans les moments de doute et m'a permis de garder le moral et la motivation jusqu'au bout. Je le remercie aussi de m'avoir offert un stage avec lui à la Seyne-sur-Mer en France et de m'avoir permis de participer au congrès de l'AGU à San Francisco.

Mes remerciements vont également à Cédric Chavanne et Natacha Bernier pour leur participation à l'évaluation de ce mémoire de maîtrise.

Ce projet de maîtrise a été rendu possible grâce au financement du ministère des Transports du Québec, que je remercie, au même titre que Québec-Océan, qui m'a offert une bourse pour participer au congrès de l'AGU à San Francisco.

J'adresse également une pensée particulière à mes parents, pour leur soutien durant ces trois ans de maîtrise au Québec, à mon père, pour avoir décelé ma passion pour l'océanographie et m'avoir encouragé dans cette voie, et à ma mère pour m'avoir donné le goût de la recherche.

Une pensée aussi pour mes très bons amis Victor et Théo, avec qui l'aventure au Québec a commencé, et sans qui je ne me serais probablement pas rendu jusque-là !

Enfin, je tiens à remercier de tout cœur toutes les formidables personnes que j'ai rencontrées à Rimouski, et qui ont fait de ces trois ans une expérience extraordinaire, autant du point de vue personnel qu'académique. Je ne les citerais pas de peur d'en oublier, mais ils et elles se reconnaitront sans aucun doute : merci les ami(e)s !

RÉSUMÉ

Avec les changements climatiques, le couvert de glace du St-Laurent tend à diminuer, laissant son littoral de plus en plus exposé à l'action des vagues, qui sont le principal facteur d'érosion côtière. La banquise a en effet un rôle protecteur en hiver, puisqu'elle atténue l'énergie des vagues et réduit le *fetch* disponible pour la génération de vagues par le vent. C'est pourquoi l'évaluation du climat de vagues à long terme dans l'estuaire et le golfe du Saint-Laurent nécessite de prendre en compte la réduction projetée de cette protection par la glace. La première partie de ce mémoire propose une méthode simple pour estimer l'évolution du couvert de glace jusqu'en 2100. Elle est basée sur de nouvelles équations empiriques entre le nombre de degré-jour de gel et les caractéristiques de la saison de glace (début, couverture maximale, durée), qui ont été définies pour le passé récent et qui sont appliquées à un ensemble de simulations climatiques de la température de l'air. L'effet du couvert de glace sur le régime de vagues durant le 21^{e} siècle est ensuite estimé en appliquant aux hauteurs de vagues un coefficient d'atténuation calculé à partir du couvert de glace. Les résultats indiquent une réduction de l'atténuation des vagues d'environ 80% pour la période 2071-2100 par rapport aux trente dernières années (1981-2010). Dans la seconde partie du mémoire, motivé par le désir de mieux représenter les processus physiques en jeu, un modèle spectral unidimensionnel de vagues prenant en compte les interactions vagues-glace et la génération par le vent est développé et utilisé pour étudier les effets de la compétition entre ces processus sur le spectre de vagues. Les résultats montrent que la répartition spatiale de la glace affecte significativement la forme et l'énergie du spectre pour des concentrations partielles entre 20% et 60% de glace.

Mots-clés : climat de vague, glace de mer, interactions vagues-glace, modèle spectral de vagues, changements climatiques, estuaire et golfe du St Laurent.

ABSTRACT

With climate change, the ice cover of the St. Lawrence tends to decrease, leaving its shoreline more exposed to the action of waves, which are the main factor of coastal erosion. Sea ice indeed has a protective role in winter, because it attenuates the wave energy and reduces the distance of open water available for the generation of waves by wind. Therefore, the evaluation of long-term wave climate in the estuary and the gulf of St. Lawrence requires taking into account the projected reduction of the ice protection. The first part of this thesis proposes a simple method to project the evolution of the ice cover until 2100. It is based on new empirical equations between the number of freezing degree-days and the characteristics of the ice season (start, maximum cover, length), which were defined using the recent past and applied on a set of climate simulations of the air temperature. The effect of the ice cover on the wave regime during the 21st century is then estimated by applying on the wave heights an attenuation coefficient computed from the ice cover. Results show a decrease of 80% of wave attenuation for the 2071-2100 period compared to the last thirty years (1981-2010). In the second part of this thesis a one-dimensional spectral wave model that takes into account wave-ice interactions and wave generation by wind is developed and used to study the competition between those processes on the wave spectrum. Results show that the spatial ice distribution significantly affects the shape and the energy of the spectrum for partial ice concentrations between 20% and 60%.

Keywords : wave climate, sea ice, spectral wave model, climate change, Estuary and Gulf of St. Lawrence.

TABLE DES MATIÈRES

LISTE DES TABLEAUX

LISTE DES FIGURES

INTRODUCTION GÉNÉRALE

Mise en contexte et problématique du projet de maîtrise

La présence de glace de mer affecte la génération et la propagation des vagues, d'une part en limitant les échanges d'énergie mécanique entre océan et atmosphère, notamment en limitant le *fetch* (Wadhams, 1983) – distance sur laquelle souffle le vent pour générer des ondes de surface– et d'autre part en atténuant l'énergie des vagues. Les observations pionnières de vagues se propageant dans la glace de Squire et Moore (1980) montrent une décroissance exponentielle de l'énergie des vagues avec la distance et suggèrent que l'atténuation est principalement due à la diffusion élastique causée par les inhomogénéités du couvert de glace (Kohout *et al.*, 2011). En effet, lorsque les vagues changent de milieu de propagation de l'eau à la glace ou de la glace à l'eau, une partie de son énergie est réfléchie, à l'instar d'une onde sonore ou lumineuse. La proportion d'énergie affectée par ce phénomène dépend, pour les vagues, de plusieurs facteurs, notamment leur période et l'épaisseur de la glace, car l'énergie des vagues diminue de manière exponentielle de la surface vers le fond de la colonne d'eau (Holthuijsen, 2007). Les vagues de longue période transportant plus d'énergie que celle de courte période, pour une épaisseur de glace donnée, la proportion d'énergie affectée par le changement de milieu de propagation est plus importante pour les courtes périodes, qui subissent donc une plus forte atténuation. De la même manière, plus la glace est épaisse, plus l'atténuation est importante. Dans le régime linéaire, le nombre d'interfaces eau-glace que les vagues rencontrent dépend donc de la taille des *floes* de glace ainsi que de leur morphologie. Les phénomènes de dissipation visqueuse (turbulence, déformation inélastiques) peuvent être importants dans certaines situations encore mal définies (Squire *et al.*, 2009). Malgré la difficulté inhérente à la collecte de telles données en milieu naturel, une étude récente basée sur une mission dans la

zone marginal antarctique a mis en évidence que l'atténuation devient plutôt linéaire lorsque les vagues dépassent une certaine hauteur (Kohout *et al.*, 2014). En tout cas, dans un contexte de changements climatiques, la disparition de la banquise laisse présager une intensification du régime de vagues, comme il a déjà été observé en Arctique (Thomson et Rogers, 2014).

Les vagues sont les principales responsables de la fracture de la glace en lui imposant une contrainte de flexion lors de leur passage (Vaughan et Squire, 2011). Lorsque la contrainte exercée par les vagues est supérieure à la contrainte maximale que la glace peut subir, elle se fracture (Squire, 1993). Cette contrainte maximale est extrêmement difficile à évaluer en milieu naturel en raison de la grande inhomogénéité de la banquise. Elle dépend de l'épaisseur de la glace, de ses propriétés mécaniques, qui sont elles-mêmes fonctions de sa salinité et de sa température, et, dans une certaine mesure, de l'historique de déformation (Timco et O'Brien, 1994 ; Langhorne *et al*., 1998). De plus, la contrainte exercée par les ondes de surface est liée à leurs caractéristiques, comme l'amplitude ou la fréquence ; plus la courbure des vagues est importante, plus la tension exercée sur la glace est importante (Bennetts *et al*., 2010). La distribution de taille des *floes* est donc fortement contrôlée par le régime de vagues (Langhorne *et al.*, 1998). Ce mécanisme de fracture de la glace intervient aussi dans les processus de formation et de fonte de la glace en accélérant la fonte latérale des floes en été, ou au contraire en favorisant la formation de glace en hiver par la création d'interstices d'eau libres entre les *floes* (Steele *et al.*, 1989; Steele, 1992; Bennetts *et al.*, 2010). Kohout *et al.* (2014) ont d'ailleurs établi une forte corrélation entre la progression ou la récession de la limite de glace et le régime de vagues dans l'océan austral.

L'étude des interactions couplées entre les vagues et la glace de mer est un sujet de recherché très actif actuellement. Cet intérêt est principalement lié à l'accessibilité accrue des régions polaires et le rôle des vagues sur la dynamique de la banquise dans des zones d'intérêt économique important, que ce soit à travers l'exploitation des ressources naturelles (pétrole, gaz, pêcheries) ou la navigation commerciale. Ces activités nécessitent une bonne connaissance de l'environnement polaire, pour garantir à la fois la sécurité des

acteurs concernés et la protection du milieu, jusque-là relativement bien préservé de l'influence anthropogénique directe. Par ailleurs, l'effet de rétroaction entre l'intensification du régime de vagues et la fonte de la banquise conduit à une action accrue des vagues sur le littoral, augmentant les risques d'érosion côtière (Overeem *et al.*, 2011).

Dans l'estuaire et le golfe du Saint-Laurent (EGSL), l'érosion côtière est une problématique qui affecte les communautés côtières, et qui pourrait s'aggraver à cause des changements climatiques (Bernatchez et Dubois, 2004; Savard *et al.*, 2009). Les vagues en sont le principal facteur, notamment lors de tempêtes hivernales, dont les effets sont d'autant plus dévastateurs lorsque la banquise n'est pas là pour protéger le littoral en atténuant l'énergie des vagues (Forbes *et al.*, 2004). Afin de prévoir les futurs risques d'érosion côtière, et de proposer des solutions adaptées pour en minimiser les impacts, il est nécessaire de caractériser le climat de vagues de l'EGSL, tâche d'autant plus ardue que la présence de glace en hiver complique considérablement le problème. Étant donné qu'il n'existe pas encore de modèle couplé vagues-glace tenant compte des processus affectant les vagues à la fois en eau libre et dans la glace, l'évaluation du climat de vagues dans le St-Laurent ne tient traditionnellement pas compte de la période hivernale (Ouellet et Drouin, 1991). Cette considération était sûrement valable il y a plusieurs décennies, mais la récente réduction à la fois spatiale et temporelle du couvert de glace saisonnier de l'EGSL en réponse aux changements climatiques (Galbraith *et al.*, 2013; Johnston *et al.*, 2005; Savard *et al.*, 2009) la rend discutable aujourd'hui.

La caractérisation du climat de vagues dans des eaux saisonnièrement couvertes de glace comme l'EGSL nécessite donc la prévision de l'évolution du couvert de glace. Pour ce faire, des modèles régionaux couplés glace-océan forcés par les solutions de modèles climatiques globaux peuvent être utilisés pour représenter de manière réaliste la dynamique des glaces. Cette méthode a néanmoins un prix élevé en ressources informatiques et restreint le nombre de simulations climatiques que l'on peut réaliser pour évaluer le climat futur de la banquise. Une simulation climatique ne représente en effet qu'une seule réalisation possible du climat, alors que la caractérisation du climat et de son évolution

nécessite plusieurs réalisations. En d'autres termes, plusieurs membres sont nécessaires pour constituer un ensemble représentatif du système climatique. Dans cette optique, une méthode empirique simple basée sur les relations significatives existant entre les principales caractéristiques du couvert de glace et des variables environnementales représente une avenue intéressante pour accomplir cette tâche, pourvu que la corrélation entre les variables soit bonne. Le concept de degrés-jour de gel a été utilisé à maintes reprises pour caractériser la sévérité de l'hiver et les conditions de glace dans les Grands Lacs (Assel, 1980) ou même en Arctique (Lebedev, 1938). Cet indicateur, que l'on définit dans le premier chapitre du mémoire, représente en fait le bilan de chaleur sensible au gré duquel la glace se forme et fond. Il ne tient toutefois pas compte de la dynamique de la banquise, comme le ferait un modèle couplé glace-océan.

La compréhension et la simulation de la complexité des interactions vagues-glace passent nécessairement par l'utilisation de modèles numériques. Plusieurs modèles d'atténuation des vagues par la glace ont vu le jour suite à l'amélioration des connaissances sur les interactions vagues-glace et à l'avancée des méthodes numériques (Kohout et Meylan, 2006, 2008; Squire *et al*., 2009; Bennetts et Squire, 2012). Ces modèles, basés sur la théorie linéaire de la diffusion des ondes par des plaques élastiques minces flottant dans un fluide non-visqueux incompressible, reproduisent bien les principales caractéristiques de la propagation des vagues dans la zone marginale (Bennetts *et al.*, 2010). Les données disponibles sont pour le moment insuffisantes pour valider ce type de modèle pour l'ensemble des conditions possibles, mais ils représentent à ce jour la meilleure théorie quantitative pour l'étude des interactions vagues-glace. Dans le cadre du projet norvégien WIFAR (*Waves-in-Ice Forecasting for Arctic Operators*), Dumont *et al*. (2011) ont proposé le *Waves-in-Ice Model* (WIM), un modèle qui intègre la théorie de l'atténuation des vagues par la glace et une paramétrisation de la fragmentation des *floes* afin de prédire la distribution de taille des *floes* dans la zone marginale à partir de l'information sur les vagues incidentes. Ce modèle donne des résultats qualitativement comparables à ce que l'on retrouve dans le détroit de Fram (Williams *et al*., 2013b). Il est de plus un outil précieux afin de mieux comprendre et modéliser des processus spécifiques dans une

optique d'implémentation des interactions vagues-glace dans des modèles numériques couplés atmosphère-glace-océan, nécessaires pour représenter la globalité des phénomènes physiques influençant la dynamique océanique.

Dans un contexte de changements climatiques, les étendues de banquise des mers du globe tendent à devenir de plus en plus éparses, laissant des étendues d'eau libre disponibles pour l'action du vent, notamment dans la zone marginale de glace arctique, ou dans l'EGSL. Le terme source de génération par le vent a donc été implémenté dans WIM afin de quantifier la compétition entre les processus d'atténuation par la glace et de génération par le vent pour un couvert de glace partiel. De plus, l'amélioration des modèles de vagues implique souvent l'amélioration de la résolution spatiale, notamment pour mieux résoudre les composantes bathymétriques et géographiques (Roland et Ardhuin, 2014). Dans cette optique, la sensibilité de WIM à la résolution spatiale a été explorée en distribuant la glace à fine échelle de différentes manières. Les résultats de cette étude constituent la deuxième partie de ce mémoire.

Ce projet de maîtrise s'inscrit dans le cadre du projet « Modélisation du régime des vagues du golfe et de l'estuaire du Saint-Laurent pour l'adaptation des infrastructures côtières aux changements climatiques » (Neumeier *et al.*, 2013) financé par le ministère des Transports du Québec (MTQ). Il s'inscrit également dans un programme de recherche plus large visant le développement de la prochaine génération des modèles environnementaux couplant atmosphère, vagues, glace et océan, appelés à constituer la base des services de prévisions opérationnels nationaux. Notamment, WIM a été inclut dans la version en développement du code WAVEWATCH III de la National Oceanographic and Atmospheric Administration (NOAA), un modèle qui est utilisé par plusieurs services opérationnels nationaux pour la prévision des vagues.

Objectifs du projet de maîtrise

Le but de ce projet de maîtrise est de quantifier les impacts des interactions vagues-glace dans l'EGSL, afin 1) d'évaluer le climat de vagues et les risques d'érosion côtière dans un contexte de réchauffement climatique et 2) d'améliorer les prévisions de l'état de la mer en présence d'un couvert partiel de glace.

Pour ce faire, les deux objectifs principaux sont :

Objectif 1 : Développer une méthode pour prévoir le climat de vagues hivernal dans l'EGSL jusqu'en 2100.

a) Établir un critère simple permettant de prévoir l'étendue spatiale et temporelle du couvert de glace dans l'EGSL ;
b) Prédire l'évolution du couvert de glace dans l'EGSL jusqu'en 2100 à partir de simulations climatiques ;
c) Évaluer l'atténuation des vagues en fonction du couvert de glace.

Objectif 2 : Améliorer la modélisation des interactions vagues-glace pour un couvert de glace partiel.

a) Implémenter la physique des processus de génération et de dissipation en eau libre dans le modèle WIM (*Waves-in-Ice Model* ; Williams *et al.*, 2013a, 2013b);
b) Caractériser l'effet de la compétition entre les processus de génération et d'atténuation des vagues dans des conditions de couvert de glace partiel ;
c) Étudier la sensibilité du modèle à la distribution spatiale de la glace à fine échelle.

Organisation du mémoire et contribution

Chacun des deux objectifs de cette maîtrise a mené à la rédaction d'un article scientifique en anglais. Ces deux articles seront soumis pour publication après le dépôt du mémoire :

L'article 1, *An empirical method to take sea ice into account for long-term wave climate forecasting in the Gulf of St. Lawrence*, présente la méthode de prise en compte de la glace pour l'évaluation du climat de vagues jusqu'à 2100. Une partie de ce travail est aussi intégrée dans le rapport remis au MTQ sur la « Modélisation du régime des vagues du golfe et de l'estuaire du Saint-Laurent pour l'adaptation des infrastructures côtières aux changements climatiques » (Neumeier *et al.*, 2013).

L'article 2, *Modeling wind generation and attenuation of waves in ice-infested waters : sensitivity to the subscale ice distribution*, présente les résultats obtenus suite à l'amélioration du modèle WIM sur la compétition entre génération de vagues par le vent et atténuation par la glace, ainsi que sur la sensibilité de ce modèle à la distribution de la glace à fine échelle.

De plus, ce projet de maîtrise m'a permis de participer à trois congrès scientifiques. Une première affiche, intitulée « Impact du couvert de glace sur le régime de vagues du Saint-Laurent », a été présentée au colloque annuel de Québec-Océan en novembre 2012, présentant les objectifs de la maîtrise. Une deuxième affiche présentant la méthode de prise en compte de la glace a été présentée au colloque de Québec-Océan en novembre 2013 : « Méthode de prise en compte du couvert de glace pour la modélisation du climat de vagues dans le St-Laurent ». Enfin, les résultats préliminaires obtenus avec WIM ont été présentés à l'AGU *Fall Meeting* à San Francisco en décembre 2013 dans une affiche Intitulée « *Modelling wave-ice interactions in the Gulf of St. Lawrence* ».

CHAPITRE I
MÉTHODE EMPIRIQUE DE PRISE EN COMPTE DE LA GLACE POUR L'ÉVALUATION DU CLIMAT DE VAGUES À LONG TERME DANS LE GOLFE DU ST. LAURENT

1.1. RÉSUMÉ EN FRANÇAIS DE L'ARTICLE I

Une méthode empirique permettant d'évaluer l'évolution du couvert de glace et son impact sur le régime de vagues hivernal dans le Golfe du St-Laurent est proposée. Pour cela, les températures de l'air à 2 m de la surface données par le modèle de ré-analyse *Canadian Global Environmental Multiscale* (GEM) ont été utilisées pour calculer le nombre cumulé de degrés-jour de gel. Les cartes de glace du Service Canadien des Glaces ont permis de calculer la couverture de glace journalière des hivers 2001-2002 à 2011-2012. Des relations empiriques ont été établies pour déterminer le début et la durée de la période d'englacement à partir de la température de l'air, ainsi que l'étendue maximale du couvert de glace. Ces relations ont été projetées à l'horizon 2100 grâce à huit (8) simulations climatiques, trois (3) provenant du Modèle Climatique Régional Canadien, et cinq (5) de la 3^{e} génération du Modèle Climatique Global Canadien, afin de déterminer l'étendue spatiale et temporelle du couvert de glace. Un coefficient d'atténuation est ensuite dérivé de la concentration de glace pour être appliqué aux sorties de modèles de vagues. Cette dernière étape constitue une partie du travail de maîtrise de Benoit Ruest, encadré par Urs Neumeier et Dany Dumont.

Cet article a été co-rédigé par moi-même et les professeurs Urs Neumeier et Dany Dumont. En tant que premier auteur, j'ai fait la revue de littérature sur le sujet, le traitement des données de températures et de glace, l'établissement des relations empiriques, et la

rédaction de l'article. L'idée d'utiliser les degré-jours de gel comme critère thermique pour la présence de glace dans l'EGSL provient de Dany Dumont, en s'inspirant des travaux d'Assel (1980) qui a établi un critère de sévérité de l'hiver pour les Grands Lacs à partir du nombre de degré-jours de gel. Urs Neumeier m'a beaucoup aidé dans le traitement des données avec le logiciel Matlab, avec lequel je n'étais alors pas encore très familier. En tant que deuxième et troisième auteurs, Urs Neumeier et Dany Dumont ont activement participé à la direction à prendre pour la recherche et la révision de l'article.

1.2. AN EMPIRICAL METHOD TO TAKE SEA ICE INTO ACCOUNT FOR LONG-TERM WAVE CLIMATE FORECASTING IN THE GULF OF ST. LAWRENCE

1.2.1. Abstract

An empirical method to evaluate the evolution of the ice cover and its impact on the winter wave climate in the Gulf of St. Lawrence is proposed. Air temperatures at 2m above sea level from the Canadian Global Environmental Multiscale (GEM) Model are used to calculate the cumulative number of freezing degree-days. Ice charts from the Canadian Ice Service are used to calculate the daily ice concentration from 2001-2002 to 2011-2012. Empirical relationships are established to determine the start and duration of the ice period, as well as the maximum ice cover. These relationships are projected to the 2100 horizon using eight (8) climate simulations, three (3) from the Canadian Regional Climate Model and five (5) from the 3rd generation of the Canadian Global Climate Model, to determine the spatial and temporal extent of the ice cover. An attenuation coefficient is then derived from the ice concentration to be applied to the outputs of wave climate projections.

1.2.2. Introduction

The Gulf of St. Lawrence (GSL) (Figure 1) is the southernmost seasonally ice-covered basin of the Northern hemisphere and experiences severe coastal erosion, mainly

caused by waves, especially during winter storms (Bernatchez and Dubois, 2004; Forbes *et al.*, 2004). Sea ice acts as a natural protection for the shoreline by reducing the fetch over which waves can grow (Wadhams, 1983) and by attenuating the wave energy along their propagation in the ice (Squire and Moore, 1980). In a context of climate change, this natural defence forms later and melts earlier in the season, leaving the coast more and more exposed to elements' wrath.

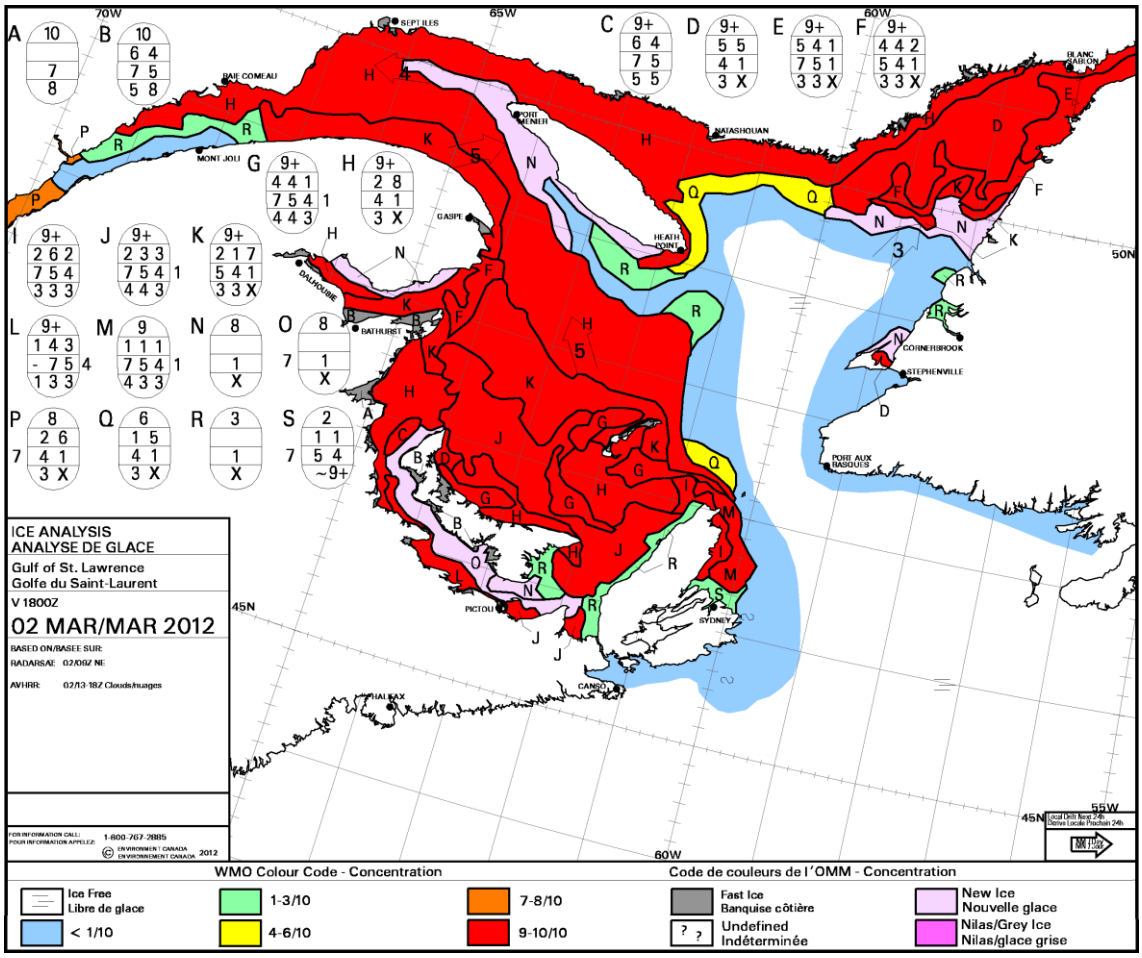

Figure 1. Ice chart from the Canadian Ice Service (CIS) of the GSL on March 2, 2012. Ice information of the different zones is given by the egg code (Fequet, 2002). The total concentration for this day is 61% in the GSL.

Informed management of coastal zones requires either long-term wave data or, when not available, long-term wave model forecasts in order to evaluate the wave climate and the return period of extreme events. This is however not trivial in sub-arctic regions during

winter because little is known about wave-ice interactions. In the GSL, coastal engineers historically did not take into account the winter season for wave climate evaluation (Ouellet and Drouin, 1991), which amounts to consider that waves were fully attenuated by ice. This assumption was perhaps reasonable a few decades ago, but recent observations of the ice season shortening and the maximum ice extent reduction in the GSL as a result of global warming (Galbraith *et al*., 2013; Johnston *et al*., 2005; Savard *et al*., 2009) make it arguable today. Another strategy could be to neglect the effect of ice during winter, which leads to the worst case scenario for coastal erosion risks. These two approaches represent two unlikely extremes of how to take ice into account for long-term wave hindcasting, so a new method between those two is proposed here.

Accurate ice forecasting can be done using regional coupled ice-ocean model simulations forced with Global Climate Model (GCM) solutions, but this comes at a relatively high computational cost mostly due to the need for solving at high resolution (~ 5 km) and the need for relatively high-resolution atmospheric climate simulations (~ 10-50 km) that adequately represent geographical features of the domain. These constraints often lead to reduce the number of simulations, which precludes the characterization of the system's inherent variability. For these reasons, we propose instead to use simplified empirical relationships based on the concept of freezing degree days (FDD) that capture most of the variability and use them to predict how the ice cover will evolve in the GSL until the 2100 horizon.

Wave attenuation is mainly attributed to ice irregularities that spread and scatter the energy at each wave-ice interface because of the difference in the dispersion relation (Kohout *et al.*, 2011). Furthermore, the attenuation coefficient depends on: the wave period, the shorter ones undergoing more attenuation than the longer ones (Liu and Mollo-Christensen, 1988; Squire, 2007); ice thickness, the thicker the ice the stronger the attenuation; and the floe size distribution, because the number of ice-water interfaces encountered by waves is a determining factor for the amount of energy removed from the waves (Perrie and Hu, 1996; Bennets *et al.*, 2010). However, this kind of wave attenuation modelling requires reliable ice thickness and floe size data that are rarely available from

long-term forecasts. A simple and robust method is to apply an attenuation coefficient, derived from the predicted ice concentration, on outputs of models that were run as if no ice were present during winter.

In this paper, we attempt to predict how the sea ice cover will evolve over the next century in the GSL and to evaluate the associated wave climate. Section 2 presents a method to estimate the main characteristics of the ice cover based solely on daily-averaged air temperature data, and a method to associate a wave attenuation coefficient to be used in conjunction with parametric wave models to evaluate the wave climate. Section 3 presents projections of the ice season characteristics for the GSL up to the 2100 horizon and the corresponding impact on wave attenuation. The method is discussed in section 4 and the main conclusions are summarized in section 5.

1.2.3. Methodology

1.2.3.1. Empirical ice prediction method

The concept of freezing degree-days (FDD) has already been used to create a winter severity index and to predict the formation of ice on the Great Lakes (Richards, 1964; Assel, 1980) or other seasonally ice-infested seas (Lebedev, 1938; Rodhe, 1952; Lee and Simpson, 1954). For example, Lebedev (1938) showed that ice thickness is roughly proportional to the square root of the cumulative FDD. Because the GSL is a marine system, the number of freezing degree-days is defined here as the departure of the daily-averaged air surface temperature from the freezing point of sea water, $T_f = -1.9°C$, where temperatures below (above) T_f are given a positive (negative) algebraic sign. The cumulative number of FDD represents essentially a measure of how cold it has been for how long, and is an indication of the net amount of heat that has been transferred from the ocean to the atmosphere through sensible and latent fluxes over a given period. When it is defined with respect to the freezing point of seawater, it indicates the proportion of heat that contributed to form sea ice. It is calculated at day n as

$$FDD_n = FDD_{n-1} - (T_n - T_f) \times 1 \text{ day} \qquad (1.1a)$$

$$FDD_n = 0 \qquad \text{if} \quad FDD_n < 0 \qquad (1.1b)$$

For the GSL, *FDD* have been calculated using air temperature 2 m above the sea surface obtained from the Canadian Global Environmental Multiscale (GEM) Model (Côté *et al*. 1998). An example of the time evolution of *FDD* is shown in Figure 2 (thick black line). From this curve we define the beginning (the first day *FDD* is persistently positive) and the end (the day *FDD* reaches its annual maximum) of winter. Digital ice charts of the Canadian Ice Service (CIS) are used to calculate the average ice concentration c (in %) over the GSL (see Figure 2, thick blue line). Based on this curve, we define the start and the end of the ice season, which are respectively the first days when the ice concentration passes above and below the minimum c_{min} threshold, and the maximum concentration c_{max}. With these three quantities we can schematize the ice season as the red triangle shown in Figure 2: the ice concentration increases from c_{min} to c_{max} between the beginning and the middle of the ice season, and it decreases from c_{max} to c_{min} between the middle to the end of the ice season.

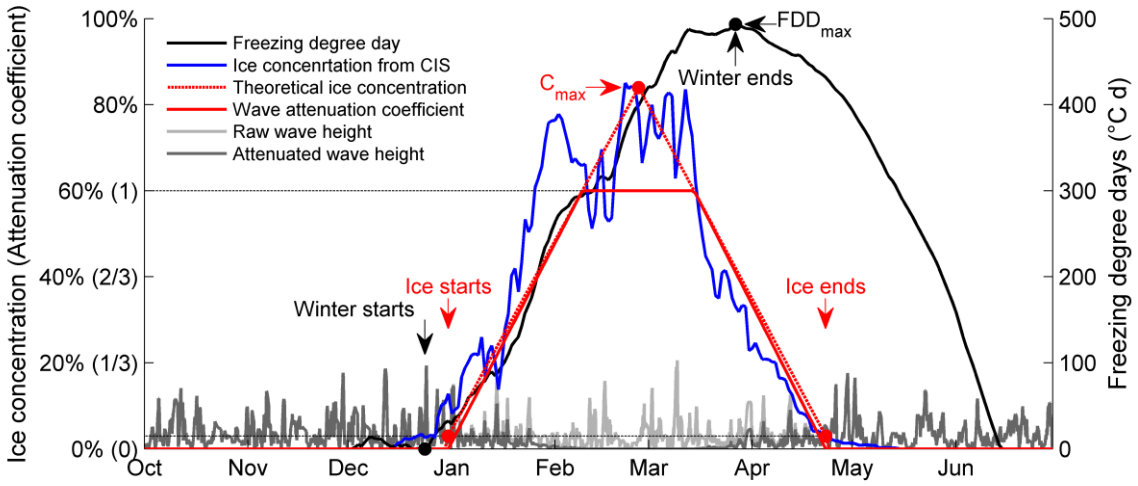

Figure 2. Schematic diagram of the wave attenuation method. The CIS ice concentration (blue) is approximated by the empirical relations from the FDD parameters (black), to obtain the theorical ice concentration (red dotted line), from which the attenuation coefficient (solid red line) is calculated. The raw wave series (light grey line) is attenuated accordingly (dark grey line).

The start and the duration of the ice season are respectively related to the start and the duration of winter by linear regressions (Equations (1.2) and (1.3)). The maximum concentration and the maximum of cumulative FDD are linked by a power regression (Equation (1.4)). The symbols used for these parameters are defined in Table 1. Figure 3 shows the correlation curve over the scatter plots of data for the 11 winters (2002 to 2012). Table 2 shows these equations, established for the period of availability of digital ice charts (2002 to 2012), and the corresponding correlation coefficients. The strong correlation between the daily calculated concentration with this procedure and the ice charts data (R^2 = 0.83) strengthens the reliability of such an empirical method to globally characterize the St-Lawrence annual ice cover. This is not surprising considering the GSL as an almost closed system where the ice freezes and melts locally, even if there is some input from the Arctic Ocean through Belle-Isle Strait and the St. Lawrence River, and some export to the Atlantic Ocean through the Cabot Strait (Hill *et al.*, 2002; Saucier *et al.*, 2003).

Table 1. Definition of symbols.

Symbol [Units]	Definition
t_{freeze} [days]	First day when $c > 3\%$
t_{start} [days]	Day when $FFD > 0$ persistently
t_{end} [days]	Day when $FDD = FDD_{max}$
l_{ice} [days]	Duration of ice period
l_{fdd} [days]	Duration of winter ($l_{fdd} = t_{end} - t_{start}$)
FDD_{max} [°C days]	Maximum of cumulative FDD
c_{max} [%]	Maximum ice concentration

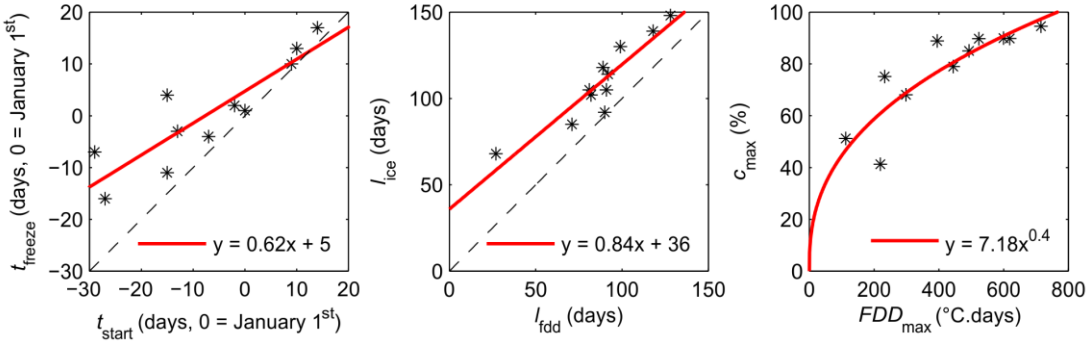

Figure 3. Scatter plots of the empirical relationships between FDD parameters and ice parameters for the beginning of winter (*left*), its duration (*middle*) and the maximum ice concentration (*right*). The black stars show the data for the 11 winters (2002 to 2012), and the red line is the correlation curve. The dotted black line is the $y = x$ curve.

Table 2. Results of the regression equations between freezing degree-days parameters and ice parameters, with corresponding correlation coefficients R^2.

Equation		R^2
$t_{freeze} = 0.62t_{start} + 5$	(1.2)	0.78
$l_{ice} = 0.84l_{fdd} + 36$	(1.3)	0.85
$c_{max} = 7.18FDD_{max}^{0.4}$	(1.4)	0.69

Eight climate simulations produced by two different models, one global and one regional, were used to project the evolution of the average ice concentration in the GSL over the 2001-2100 period using the empirical relationships. All simulations follow the IPCC SRES A2 scenario (Nakicenovic *et al.*, 2000). Five simulations come from the

Canadian Global Climate Model (CGCM) 3rd generation and three simulations come from the Canadian Regional Climate Model (CRCM) version 4.2.3 (Table 3). The three regional simulations are called CRCM-ahj, forced by the 3rd member of ECHAM5, CRCM-aev forced by the 5th member of CGCM3.1, and CRCM-aev-unbiased that was unbiased for temperatures using the quantile method (Anandhi *et al.*, 2011) by Senneville *et al.* (2013). The regional simulations cover the period 1961-2100, but the global simulations only cover the period 2001-2100.

Table 3. Description of climate simulations used to project the average ice concentration.

Simulation	Model	Member	Driver	Period
1	CRCM 4.2.3	ahj	ECHAM5	1961-2100
2	CRCM 4.2.3	aev	CGCM 3.1	1961-2100
3	CRCM 4.2.3	aev-unbiased	CGCM 3.1	1961-2100
4	CGCM 3.1	member 1	-	2001-2100
5	CGCM 3.1	member 2	-	2001-2100
6	CGCM 3.1	member 3	-	2001-2100
7	CGCM 3.1	member 4	-	2001-2100
8	CGCM 3.1	member 5	-	2001-2100

The 2-m surface temperatures of the Modern-Era Retrospective Analysis for Research and Applications (MERRA) (Rienecker *et al.*, 2011) are used to define a 30-year reference climate for the period 1981-2010. A second order polynomial correction has been applied to MERRA temperatures to better fit with GEM, which we consider is the best product for air temperatures in the GSL but which is not available over a sufficiently long period.

1.2.3.2. Wave attenuation post-processing

Wave conditions in ice-infested waters result from many processes acting together and affecting their generation, propagation and dissipation. For the purpose of evaluating climatic conditions over a large basin, we continue to adopt a simple parameterization of the effect of sea ice on wave conditions based on the crude fact that the more sea ice there

is, the less waves there are. The simplest mathematical representation of this statement is to devise a wave attenuation coefficient α between 0 and 1 that will be applied to the significant wave height determined in the absence of ice. We thus assume that there will be no wave if the ice concentration is above a threshold c_{max} and that waves won't be affected if the ice concentration is below c_{min} = 3%. Between c_{min} and c_{max}, we assume a linear function of the daily averaged ice concentration c_n. The attenuation α_n for day n is then given by

$$\alpha_n = \begin{cases} 0 & \text{if } c_n < c_{min} \quad (1.5a) \\ \frac{c_n - c_{min}}{c_{max} - c_{min}} & \text{if } c_{min} < c_n < c_{max} \quad (1.5b) \\ 1 & \text{if } c_n > c_{max} \quad (1.5c) \end{cases}$$

Figure 4 shows how the attenuation coefficient varies as a function of the averaged ice concentraiton with c_{min} = 3% and c_{max} = 60%. A sensitivity analysis of the c_{max} value is presented in the discussion section.

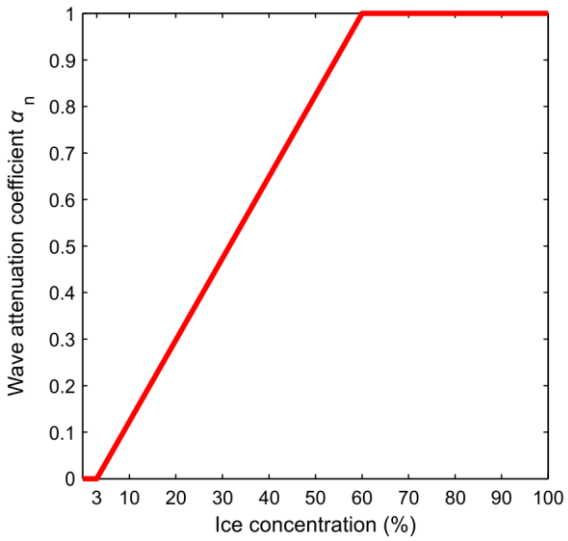

Figure 4. Wave attenuation calculated from ice concentration, with c_{min} = 3% and c_{max} = 60%.

The significant wave heights calculated by a wave model have to be multiplied by the attenuation factor $(1 - \alpha_n)$ for the whole ice period. The waves then experience attenuation proportional to the ice concentration, as it is shown schematically in Figure 2.

Similar approaches are used in wave models that take into account sea ice. In their study for wave forecasting in the seasonally ice covered Baltic Sea, Tuomi *et al.* (2011) treated the 5-km grid cells of their model in which the ice concentration exceeded 30% as land point. If the ice concentration was lower than this threshold, the cell was considered as open water. Tolman (2003) did the same with a cut-off concentration of 33%. At these values, our parameterization attenuates waves by about half.

1.2.4. Results

1.2.4.1. Climate change perturbations on GSL sea ice

Climate changes affect both the duration of the ice period and the amount of ice formed during winter. Figure 5 shows the ensemble-averaged (eight simulations) ice concentration and the trends of the duration of the ice period and the maximum ice concentration reached yearly. The color patches represent one standard deviation around the mean for the eight simulations for 2001-2100, but only for four simulations for 1981-2001 (three from CRCM and one from MERRA).

All eight climate simulations used to predict the ice cover suggest a substantial shortening of the ice period. The 1981-2010 reference ice climate indicates an average ice period of 112 days whereas the average length for 2071-2100, calculated from the mean of all eight simulations is 65 (±15) days. A decrease of the maximum ice concentration is also predicted by all simulations, from an average of 70.1% for the reference climate to 28.4 (±10.3) % for the average future climate. This represents a loss of approximately 9.8×10^4 km² for the maximum ice coverage. Furthermore, the 60% threshold for ice concentration, beyond which we consider waves are fully attenuated, won't be reached anymore after 2059 (±14 years). The last winter when such a concentration is attained is 2077, in

simulation 6. This means there is not a single day after 2077 during which waves are fully attenuated, according to these simulations.

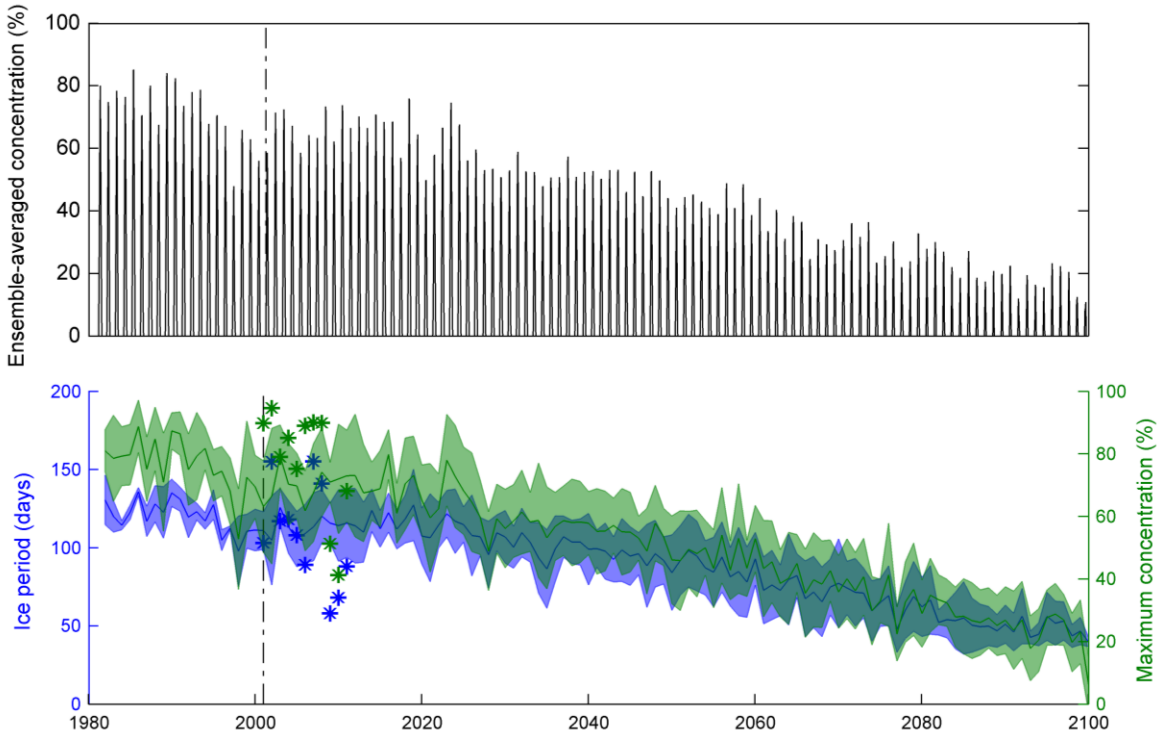

Figure 5. Evolution of the ice cover. *Top.* Daily ice concentration averaged on the eight climate simulations. *Bottom.* Mean (thick line) and standard deviation (color patch) of the ice period (blue, in days) and the maximum ice concentration (green, in %) averaged on the eight climate simulations. The vertical dotted black line shows the start of availability of the 5 CGCM members. Only 4 simulations are taken into account before this line (3 from CRCM and 1 from MERRA) while eight simulations are used after (CRCM and CGCM). The stars represent the data for the 11 winters used to establish the empirical relationships.

1.2.4.2. Wave attenuation

Both the shortening and the decrease of ice cover have consequences on wave attenuation, being less effective and on a shorter period. Figure 6 shows the daily attenuation coefficient calculated from simulations 1, 2 and 3, and the corresponding yearly coefficient *A*, calculated as the sum of the daily coefficient over the winter:

$$A = \sum_n \alpha_n \quad \text{[days]} \tag{1.6}$$

The trend of A reflects the evolution of the total impact of ice cover on the seasonal wave climate by taking into account both the ice period and the amount of attenuation. The average yearly coefficient for the MERRA reference ice climate is 64, whereas it is 71 for simulation 1, 63 for simulation 2 and 78 for simulation 3 during the same period. These three values respectively fall to 7.1, 6.1 and 21 for the 2071-2100 period, representing a reduction of the total impact of ice of 90%, 90% and 73% respectively, or 84% in mean. This suggests the impact of ice on the wave regime will be four to ten times (six times in mean) less effective in the future period (2071-2100) compared to the recent past (1981-2010).

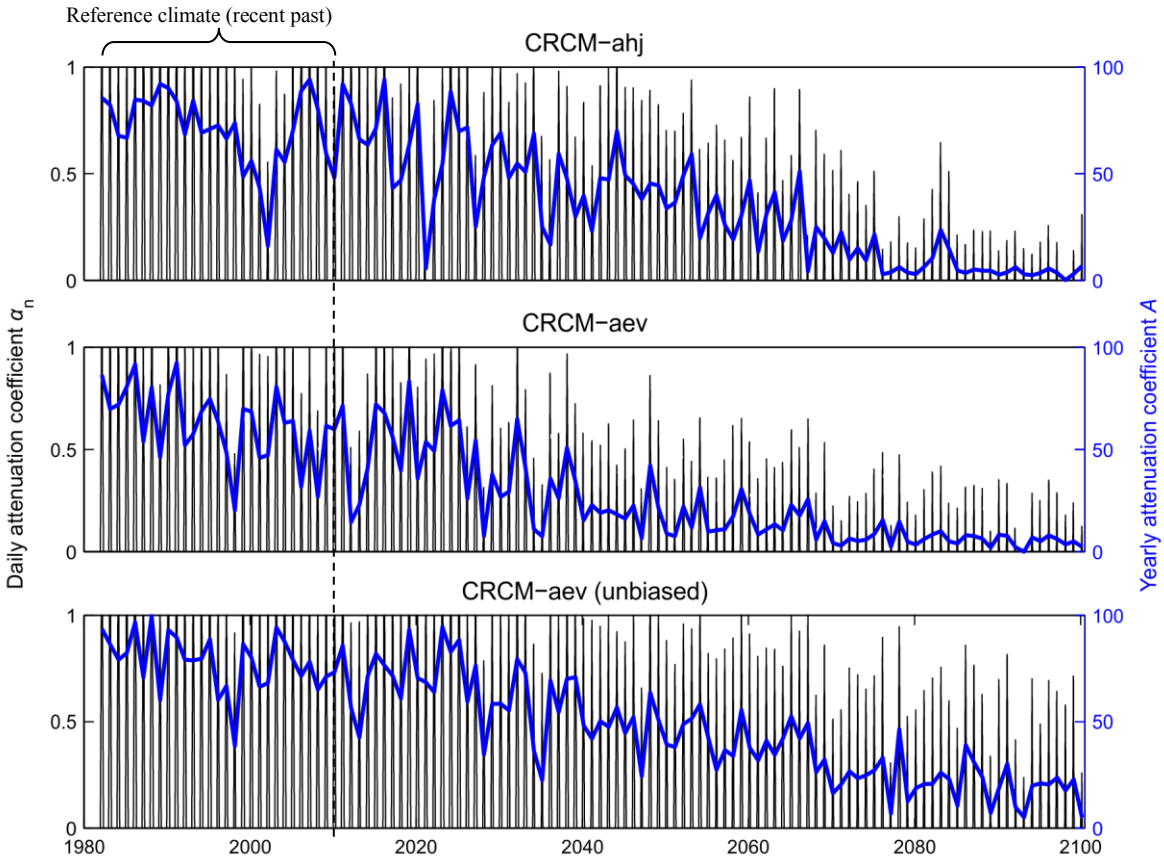

Figure 6. Evolution of the daily attenuation coefficient α_n (black curve) and the yearly attenuation coefficient A (thick blue line), for the 3 CRCM simulations used to calculate the wave attenuation.

1.2.5. Discussion

Equations (1.2), (1.3) and (1.4), which link FDDs to the ice cover, bear acceptable physical meaning. Equation (1.2) indicates that t_{freeze} and t_{start} are equal on January 14th. Before this date, cold temperatures precede ice formation by the time air cools the water trough sensible heat fluxes, a mechanism that can be slowed by water convection, and by the time water changes state, which is not instantaneous either. After January 14th, some ice appears in the GSL before the winter starts. A plausible explanation for this is that the presence of sea ice in the GSL depends on some level to what happens in adjacent connected water bodies, like the Labrador Sea and the St. Lawrence River. Considering this, it is likely that some inputs of arctic or freshwater ice occur even if the air is not cold enough above the GSL to locally freeze the water. Equation (1.3) indicates that the ice remains in the GSL approximately 30 days longer than the duration of winter. This makes sense knowing that the melting process can be, like the freezing, quite long, depending on ice density and thickness, even if the air temperature is positive. The power regression equation (1.4) is inspired from Lebedev (1938), who linked the ice thickness to the FDD using a power law. This choice ensures that for a null cumulative FDD value, the maximum ice concentration is zero. As we expect the GSL to experience warmer winters in the future, and very few data is available to characterize such winters until now, the utilization of a power regression that converges to zero gives adequate results for ice concentration when the cumulative value of FDDs is small.

Also these climate relationships assume the stationarity of the ice regime. For example, the ice formation in the GSL is strongly dependent on the Cold Intermediate Layer (CIL), which has experienced erosion these last few years (Galbraith, 2006). One of the shifts in the global GSL mechanisms that could disturb the ice formation is the disappearance of the CIL, in which case such a characterization of the ice climate may no longer be valid. Nevertheless, ice concentration predictions from the FDD empirical method are compared (Figure 7) to the outputs of the Regional Oceanic Model (ROM) with ice formation, dynamic and melting implemented by Senneville *et al.* (2013) for the GSL.

This coupled ocean-atmosphere model has been run only for two CRCM simulations (CRCM-ahj and CRCM-aev (unbiased)), so the validation of the empirical method only concerns these two simulations.

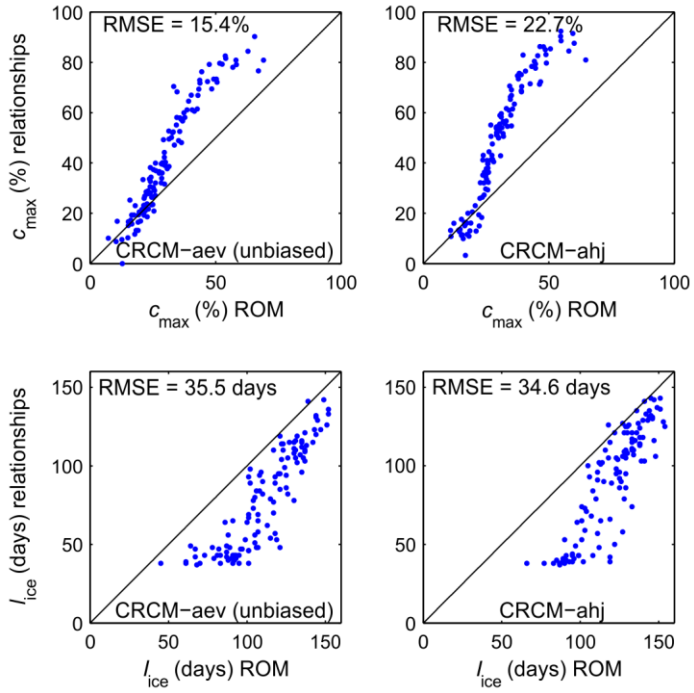

Figure 7. Comparison between the ice parameters obtained by the empirical relationships and ROM (Senneville *et al.*, 2013). The Root Mean Square Error (RMSE) is indicated in the top left of each panel. *Top* : maximum ice concentration for CRCM-aev (unbiased) (*left*) and CRCM-ahj (*right*). *Bottom* : length of ice period for CRCM-aev (unbiased) (*left*) and CRCM-ahj (*right*).

The correlation is quite good for the low values of c_{max}, and validates the choice of using a power regression to calculate it, even if it overestimates the high values of c_{max}. This has to be taken into account, but the good correlation for warm winters validates the utilization of the empirical prediction method to characterize the long-term ice climate in a context of global change. However, the ice period is underestimated by the empirical relationships compared to the model, especially for short winters, which is more problematic to characterize the future ice climate in a context of global warming. Nonetheless, the correlation is satisfying with regard to the simplicity of the empirical method. ROM reproduces the thermodynamics processes of sea ice but requires a lot of

computing resources and time, whereas the FDD method gives results quickly and with little computing resources.

The advantage of such a rapidity of execution lies in the large number of atmospheric simulations we can use to predict future ice conditions and the statistically robust wave climate derived from it. Eight simulations have been used to predict ice formation, but only three from the regional CRCM are used to calculate wave attenuation. This choice is a matter of spatial resolution. Because the resolution of the global CGCM (approximately 415 × 280 km at 48°N) is too coarse to adequately represent the wind fields at the scale of the GSL, it should not be used as a forcing of any wave model, whereas the finer resolution of the CRCM (45km × 60km at 48°N) is more adapted for such a purpose. In order to stay consistent, it seems appropriate to use the same atmospheric forcing for both wave and ice forecasting, even if spatial resolution does not affect the average air temperature used for the ice prediction method as much as the wind field used as wave model forcing. This is the reason why only the three CRCM simulations have been used to calculate wave attenuation.

Two assumptions are made for wave attenuation. Firstly, to calculate one daily attenuation coefficient for the whole GSL amounts to consider ice spatial distribution has no effect on wave attenuation. This assumption constitutes the main limitation of the method considering the results of Chapter II of this thesis, which shows that ice spatial distribution can strongly affect wave attenuation in conditions of wind blowing over a partially ice-covered region. Although this assumption simplifies wave behaviour in presence of ice, it is necessary to keep this method simple given the high computational cost and the inaccuracy of long-term climate simulation. Secondly, the same attenuation is applied to all waves regardless to their period, which means the complexity of waves-ice interactions are not taken into account. Nevertheless, ice affects the wave climate in two different ways; the formation of long waves is limited by fetch reduction (Wadhams, 1983), especially in a semi-closed sea like the GSL where waves are locally generated, and short waves are preferentially attenuated when propagating through ice (Liu and Mollo-

Christensen, 1988; Squire, 2007). Considering these two processes have an equivalent effect on the energy of short and long waves, it is not so inappropriate to attenuate waves of all periods the same way. Once again, this assumption is made to simplify the method. The alternative would be to use coupled waves-ice models that we consider still not suitable for climate purpose given the actual limited understanding and the difficulty to accurately model waves-ice interactions.

The daily attenuation coefficient is calculated empirically from the average ice concentration in the GSL, in a linear way between 0 if there is less than c_{min} = 3% and 1 if the concentration is higher than c_{max} = 60%. The 3% criterion gives the best correlation for equations (1.2) and (1.3). At such concentration, it is very likely that the ice cover will be located very close to the shoreline or at the head of small bays and will not affect waves very much. Figure 1 shows the GSL covered by 61% of ice, and the ice cover appears to be extended enough to prevent the existence of waves along most coastal areas except western Newfoundland. Nonetheless, a sensitivity study was made to quantify the effect of the arbitrary criterion c_{max} on the averaged yearly attenuation coefficient, with values of c_{max} = 50% and c_{max} = 75% (Figure 8). The wave-attenuation variability associated to this parameter is of the same order of magnitude than the variability between simulations. On the other hand, the averaged yearly coefficient A decreases the same from the recent past to the future, independently of c_{max}. Indeed, this decrease varies between the three cases from 1.3%, 1.1% and 4.8% for simulations 1, 2 and 3 respectively, which means the choice of this parameter has low impact on the reduction of wave attenuation throughout the century.

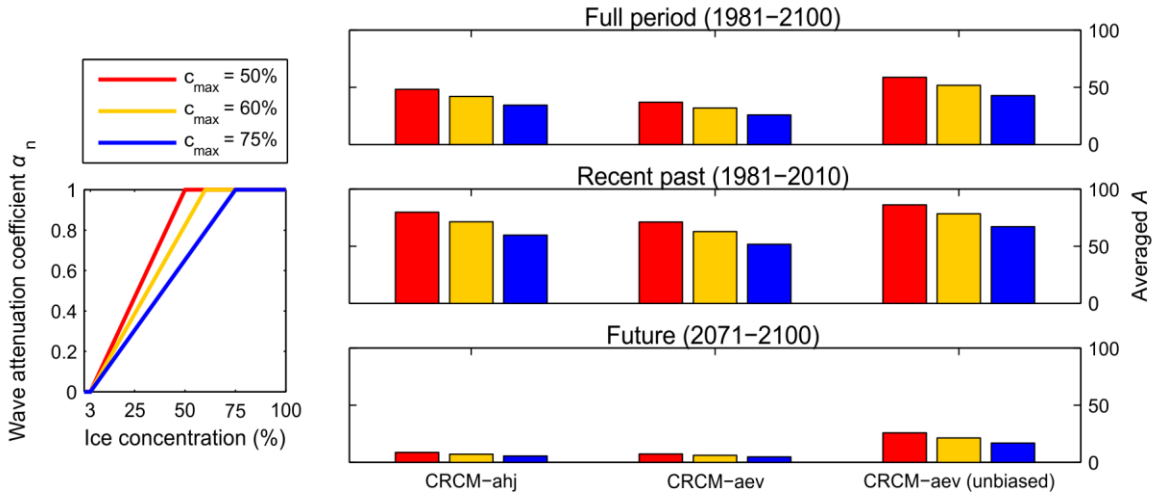

Figure 8. Sensitivity study on the choice of c_{max} for c_{max} = 50% (red), c_{max} = 60% (yellow) and c_{max} = 75% (blue). Left panel shows the attenuation coefficient calculated from ice concentration. The three right panels show the yearly coefficient A averaged for the full period (*top*), the recent past (*middle*) and the future (*bottom*), for the three CRCM simulations for each c_{max}.

1.2.6. Conclusion

A simple method to forecast future ice cover in the Gulf of St. Lawrence is presented. Freezing-degree days are used as a proxy to estimate when the ice period starts and ends, and what will be the maximum ice coverage, using air temperature and ice concentration for the last 11 years (from 2002 to 2012). The empirical relationships found to link FDD to ice parameters are projected to the 2100 horizon using 8 climate simulations. The forecasted future ice cover is used to define an attenuation coefficient for wave model outputs, that only take into account the ice concentration, regardless of the wave period or the ice thickness, that are both known to be the most important factors for wave attenuation by ice. Despite the several limitations of this method, it provides a simple method for statistical wave forecasting in seasonally ice-infested waters like the GSL.

The results lead to predict a substantial loss of ice cover throughout the century, with both the maximum ice concentration and duration of ice period being halved by 2100. This means waves will be much less attenuated during winter, by about 80%, leaving the

shoreline defenseless facing the winter storms that can already be very destructive. These results match other studies that foresee an increase in coastal erosion risk in Arctic (Overeem, 2011) due to ice cover reduction.

Even if only 3 members have been used to calculate an attenuation coefficient, the interest of such a method lies in the large number of simulations that can be used to predict the ice cover, leading to a statistical estimate of future ice regime. Furthermore, the empirical relationships can be updated every year with new ice and temperature data. This is a simple but interesting alternative to the usual way of forecasting ice cover with resource intensive models.

1.2.7. Acknowledgments

This study was funded by the Government of Québec (Ministère des Transports du Québec). Simon St-Onge-Drouin and Simon Senneville are greatly acknowledged for the outputs of their ice model. We also want to thank James Caveen for his technical support.

CHAPITRE II
MODÉLISATION DE LA GÉNÉRATION PAR LE VENT ET DE L'ATTÉNUATION DES VAGUES EN EAUX COUVERTES DE GLACE : SENSIBILITÉ À LA DISTRIBUTION DE LA GLACE À SOUS-ÉCHELLE

2.1. RÉSUMÉ EN FRANÇAIS DE L'ARTICLE II

La banquise affecte la génération et la propagation des vagues en réduisant le *fetch* et en atténuant leur énergie. Dans un contexte de changements climatiques, les couverts de glace deviennent plus épars, laissant de larges bandes d'eau libre disponibles pour l'action du vent. Étant donné que l'atténuation par la glace et la génération par le vent en eau libre sont fortement sélectifs en fréquence et non linéaires, la compétition entre ces deux termes peut mener à des différences significatives dans le spectre des vagues selon la répartition spatiale de la banquise. Pour étudier cette hypothèse, le terme source de génération par le vent a été ajouté à un modèle d'atténuation des vagues par la glace. Cette étude montre que sous certaines conditions, le vent peut générer des vagues au sein d'un couvert de glace partiel. De plus, la sensibilité du modèle à la distribution de la glace à fine échelle a été étudiée, et montre que la compétition entre l'atténuation et la génération est très dépendante de cette distribution.

Cet article a été co-rédigé par moi-même et les professeurs Urs Neumeier et Dany Dumont. En tant que premier auteur, j'ai fait la revue de littérature, l'implémentation et la documentation des processus d'eau libre dans le code du modèle, ainsi que les simulations

faites avec ce modèle. Dany Dumont m'a aidé à me familiariser avec le modèle, qu'il a lui-même développé dans le cadre du projet WIFAR (Dumont *et al.*, 2011), et a donné l'idée originale d'étudier le comportement des vagues pour un couvert de glace partiel en incluant l'effet du vent. Il m'a aussi beaucoup conseillé quant à la direction à suivre pour cette étude. Urs Neumeier a quant à lui aidé à l'optimisation du code du modèle afin de le rendre plus efficace. Tous deux ont aussi participé activement à la révision de l'article.

2.2. MODELLING WIND GENERATION AND ATTENUATION OF WAVES IN ICE-INFESTED WATERS : SENSITIVITY TO THE SUBGRID ICE DISTRIBUTION

2.2.1. Abstract

Sea ice affects the generation and propagation of ocean waves by reducing the fetch and attenuating their energy. In a context of climate change, the ice cover in ice-infested seas becomes sparser, leaving bands of open water free for the wind to blow over. As the competition between the attenuation by ice and the generation by wind in open water has so far received little attention, we explore the implementation of the wind input source term in a waves-in-ice model. This study shows that under certain circumstances, the wind can generate waves inside a partial ice cover. Furthermore, the sensitivity of this model to the subgrid ice distribution is tested, and shows that the competition between attenuation and generation is strongly affected by the way ice is distributed at fine scale.

2.2.2. Introduction

With the climate warming and the ice rapidly decreasing in the Arctic Ocean, new perspectives for commercial activities are envisaged, like oil exploitation and navigation. At the same time, larger ice-free areas also mean that higher seas and swell can be generated. Thomson and Rogers (2014) report that swell of up to 5-m significant height can be generated in the western Arctic when storm winds blow over large ice-free areas open as

a result of the ice extent decline. Spectral wave models such as WAVEWATCH III (Tolman *et al.*, 2014), used by Thomson and Rogers (2014), or WAM (WAMDI group, 1988) constitute a key part of operational monitoring and forecasting systems and have become essential planning tools for maritime operators. These models are also increasingly used to evaluate the risk of coastal erosion in a context of climate change. However, their use in ice-covered seas is limited due to a poor representation of wave-ice interaction processes.

When waves propagate in ice-covered seas, a portion of their energy is scattered more or less in every direction by inhomogeneities of sea ice (floe edges, ridges, cracks), resulting in a progressive attenuation of the energy propagating forward into the ice (Squire *et al.*, 1995; Squire, 2007). This attenuation strongly depends on the wave period (Squire and Moore, 1980; Liu and Mollo-Christensen, 1988; Squire *et al.*, 2009) as a result longer waves propagate longer distances. Attenuation also depends on the ice thickness and floe size, but more generally on the heterogeneity of the ice cover (Perrie and Hu, 1996; Kohout and Meylan, 2008; Kohout *et al.*, 2011; Bennetts *et al.*, 2010).

Many models were developed to simulate how waves are attenuated when they propagate through sea ice. These models can be classified into two categories: scattering models and viscous models. The former consider sea ice as a collection of thin elastic plates that redistribute conservatively the energy of a plane wave in all directions. In this case, wave attenuation is the ratio of the transmitted to incident wave energy in the direction of the incident wave. Variants of such models have been proposed (Kohout and Meylan, 2006, 2008; Squire *et al.*, 2009; Bennetts and Squire, 2012) and represent well the main features of waves propagating in the marginal ice zone (Bennetts and Squire, 2012). Viscous models consider the ice layer as a suspension of solid particles in water, resulting in a viscous layer lying over an inviscid fluid (Keller, 1998; De Carolis *et al.*, 2005). In this case, waves lose energy through dissipative processes as they propagate in ice-covered waters. Such models compared well with laboratory data of wave attenuation and dispersion in grease ice or frazil (Newyear and Martin, 1999), but have a limited

application for solid ice floes conditions. There is currently no comprehensive model describing the propagation of gravity waves into all types of ice cover (Wang and Shen, 2010).

Flexural movements of ice induced by waves exert a strong control on the floe size distribution (Squire, 1993; Vaughan and Squire, 2011), which in return affects the wave scattering field and, consequently, the attenuation. Dumont *et al.* (2011) developed a one-dimensional waves-in-ice scattering model (WIM) to study how these two processes, wave attenuation and floe breaking, act together to determine the extent of the marginal ice zone and its wave-induced floe size distribution. Their model, further modified, characterized and tested by Williams *et al.* (2013a, 2013b), is in fact a very simplified spectral wave model where the only source term is the attenuation due to the ice. Attenuation coefficients used in WIM are pre-computed as a function of wave period and ice thickness using various approximations of the thin elastic theory (Kohout and Meylan, 2008; Squire *et al.*, 2009; Bennetts *et al.*, 2010; Bennetts and Squire, 2012).

In its original formulation, WIM did not take into account wind generation and growth as source terms. Nonetheless, wind can significantly transform the wave spectrum in partially ice-covered conditions, typical of Arctic and Antarctic marginal ice zones and seasonally ice–covered seas. Furthermore, the improvement of wave models often requires increasing the spatial resolution (Roland and Ardhuin, 2014), for example to better resolve bathymetric and geographic features. A particularly relevant aspect for wave-ice interactions is the horizontal distribution of sea ice. Ice-ocean models as well as satellite-based sensors represent partial sea ice cover as a well-mixed combination of open water and sea ice, irrespective of the subgrid scale distribution, while in fact, and especially in presence of waves, sea ice arranges in narrow bands, filaments, clusters of floes or polynyas (Wadhams, 1973; Hermann, 2012). The horizontal distribution of sea ice is however determinant for wave dynamics: it controls how wind-wave generation and attenuation, two non-linear processes, act and compete against each other to shape the wave spectrum.

In this paper, we modify WIM and characterize its sensitivity to subgrid scale ice distribution in order to better assess the uncertainty arising from the competition between generation by wind and attenuation by ice in ice-infested seas. Section 2 provides a description of the model, section 3 presents the method to characterize these two competing processes and to quantify the sensitivity of WIM to the subscale ice distribution. Results are presented and discussed in section 4 and the main conclusions are summarized in section 5.

2.2.3. Model description

In its previous version, described in detail by Williams *et al.* (2013a, 2013b), WIM is a one-dimensional phase-averaged spectral wave model designed to study the combined effects of wave attenuation by sea ice and the ice breaking by waves. A incident wave spectrum E_{initial} is required as input, as well as ice properties along a deep ocean transect, namely ice thickness (h_i), concentration (f_i) and floe size (D) averaged over cells of a few kilometers length. Here, we add two terms to the evolution equation, namely the generation by wind S_{in} and the dissipation by white-capping S_{wc}, weighted by the fraction of open water within a cell ($1 - f_{\text{i}}$), yielding the governing equation

$$\frac{1}{c_{\text{g}}} \mathrm{D}_t E = (1 - f_{\text{i}})(S_{\text{in}} + S_{\text{wc}}) + f_{\text{i}} S_{\text{ice}} \qquad (2.1)$$

where c_{g} is the wave group speed, and $\mathrm{D}_{\text{t}}E$ is the material derivative representing the advection of the one-dimensional wave energy spectrum $E(\omega, x, t)$. S_{ice} is the ice attenuation term weighted by the fraction of ice f_{i}. White-capping is added to limit the growth of short waves in long stretches of open water between ice-covered areas. Floe breaking is neglected in the WIM-version used here and ice properties, except concentration, are kept constant throughout the study. This choice is made to place the focus on quantifying the sensitivity to the ice spatial distribution. The governing equation is solved by sequentially computing the advection and source terms on a discretized space and time. The advection is performed over the whole transect every time step before the three

source terms are calculated. The wave spectrum is updated with the wind input before the negative source terms are applied. An explicit scheme is used to integrate the positive source terms whereas the negative ones are computed implicitly (Booij *et al.*, 1999). Each of these steps is presented below.

2.2.3.1. Advection

The advection step

$$\frac{1}{c_{\mathrm{g}}}\mathrm{D}_t E(\omega, x, t) = 0 \tag{2.2}$$

is solved using a Lax-Wendroff scheme with a Superbee flux limiter for each cell as in Williams *et al.* (2013a, 2013b). This type of numerical scheme is stable and occasions very low numerical diffusion. The time step Δt is chosen so that the faster waves (i.e., the low-frequency ones) travel one cell per iteration

$$\Delta t = \frac{\Delta x}{c_{\mathrm{g}}^{max}} \tag{2.3}$$

where $c_{\mathrm{g}}^{\max}$ is the maximum group speed and Δx is the grid spacing.

2.2.3.2. Generation by wind

From Phillips (1957) theory, the general form for the wind input is

$$S_{\mathrm{in}} = a + bE \tag{2.4}$$

where a represents the wave initial growth from a calm sea, which becomes rapidly negligible as the waves start to grow exponentially from the wave-induced wind-pressure variation as the wind blows over an already existing wave field. Since we consider a non-zero incident wave spectrum, this term is neglected. The exponential growth term bE is taken from Snyder *et al.* (1981) and Komen *et al.* (1984) and is adapted for a 1-dimensionnal spectrum with the wind blowing in the direction of the wave propagation. It is given by

$$b = 0.25\omega \frac{\rho_a}{\rho_w}(28\frac{u_*}{c_p} - 1) \quad (2.5)$$

where ω is the radial frequency, ρ_a and ρ_w are respectively the air and water densities, c_p is the phase speed and u_* is the friction velocity converted from the 10m wind speed U_{10} following (Wu, 1982)

$$u_* = \begin{cases} U_{10}\sqrt{1.2875 \times 10^{-3}} & \text{for } U_{10} < 7.5 \text{ m s}^{-1} \quad (2.6a) \\ U_{10}\sqrt{(0.8 + 0.065U_{10}) \times 10^{-3}} & \text{for } U_{10} \geq 7.5 \text{ m s}^{-1} \quad (2.6b) \end{cases}$$

2.2.3.3. White-capping

Hasselman (1974) gave to the white-capping term the general form

$$S_{wc} = -\mu k E \quad (2.7)$$

where k is the wavenumber and μ is a coefficient expressed in terms of integrals over the whole spectrum (Bouws and Komen, 1983 ; Komen *et al.*, 1984)

$$\mu = 2.36 \times 10^{-5} \left(\frac{\tilde{s}}{s_{PM}}\right)^4 \frac{\tilde{\omega}}{\tilde{k}} \quad (2.8)$$

where the overall steepness $\tilde{s}$ (Janssen, 1991; Günther *et al.*, 1992) is defined as $\tilde{s} = \tilde{k}\sqrt{m_0}$, where m_0 is the 0th order moment of the spectrum, and $s_{PM} = \sqrt{3.02 \times 10^{-3}}$ is the value of $\tilde{s}$ for the Pierson-Moscovitz spectrum for a fully developed sea (Pierson and Moscovitz, 1964). The mean frequency ($\tilde{\omega}$) and mean wavenumber ($\tilde{k}$) are defined as (WAMDI group, 1988)

$$\tilde{\omega} = \left[m_0^{-1} \int_0^{\infty} \omega^{-1} E(\omega) d\omega\right]^{-1} \quad (2.9a)$$

$$\tilde{k} = \left[m_0^{-1} \int_0^{\infty} k^{-1/2} E(\omega) d\omega\right]^{-2} \quad (2.9b)$$

These integrals are numerically solved using the trapeze method.

2.2.3.4. Attenuation by ice

The attenuation source term is simply parameterized as

$$S_{\text{ice}} = -\alpha E \tag{2.10}$$

where

$$\alpha = \underline{\alpha}\frac{1}{\langle D \rangle} \tag{2.11}$$

is an attenuation coefficient with units of m^{-1} and $\langle D \rangle$ the average floe size. $\underline{\alpha}$ is an adimensional attenuation coefficient that specifies the amount of energy scattered back per floe. It is a function of the ice thickness and wave frequency and is calculated following the method of Kohout and Meylan (2008). This method consists in calculating the fully-coherent scattering response of a large number of randomly distributed ice floes modeled as thin elastic plates. A refinement to this method has been proposed by Bennetts and Squire (2012) who chose to randomly vary the phase instead of the floe separation, thus increasing the efficiency of the calculation. Since our goal is mainly to study the sensitivity of the model, the choice of the scattering model used to pre-compute α is not crucial, so the formulation of Kohout and Meylan (2008) was retained.

As a final step, the limiter $\Delta S_{\max}$ is set to limit the maximum total change of action density per iteration at each discrete frequency (Holthuijsen, 2007), in order to suppress the development of numerical instabilities, especially for high frequency waves.

$$\Delta S_{\max} = \frac{8.1\times10^{-4}}{2\omega k^3 c_{\text{g}}} \tag{2.12}$$

2.2.4. Method

As mentioned earlier, the main goal of this study is to quantify the competition between the wave generation by wind and the attenuation by ice inside the finest resolution

used presently in the Canadian Operational Ice-Ocean Model (Smith *et al.*, 2013) in the GSL (5 km), and to study the sensitivity of this model to the subscale ice distribution. The 5-km resolution is also the scale, at which ice data is given in ice charts of the Canadian Ice Service. For this study, a transect of length $X = 5$ km is subdivided into $n_x = 10$ sub-cells of length $\Delta x = 500$ m. A value of ice concentration from $f_i = 0$ to $f_i = 1$ is attributed to the whole 5-km transect.

Two different ice distributions are considered (Figure 9). The first one is the homogeneous partial ice cover, for which all sub-cells are given the same concentration f_i^* such as the concentration is f_i over the whole transect, i.e. $f_i^* = f_i$ (Figure 9, middle top panel). In this case, WIM solves the governing equation (2.1) in each sub-cell. This ice distribution is used to study the competition between open-water and ice processes in state-of-art models of waves in ice. The second ice distribution intend to quantify the sensitivity induced by the ice distribution; we use a binary ice distribution, where $n_i = n_x f_i$ sub-cells are assigned a value of concentration $f_i^* = 1$, whereas the other $n_x - n_i$ sub-cells are given a concentration $f_i^* = 0$ so that the total concentration f_i of the whole transect is the same with totally ice covered sub-cells and open water ones (Figure 9, two middle bottom panels).

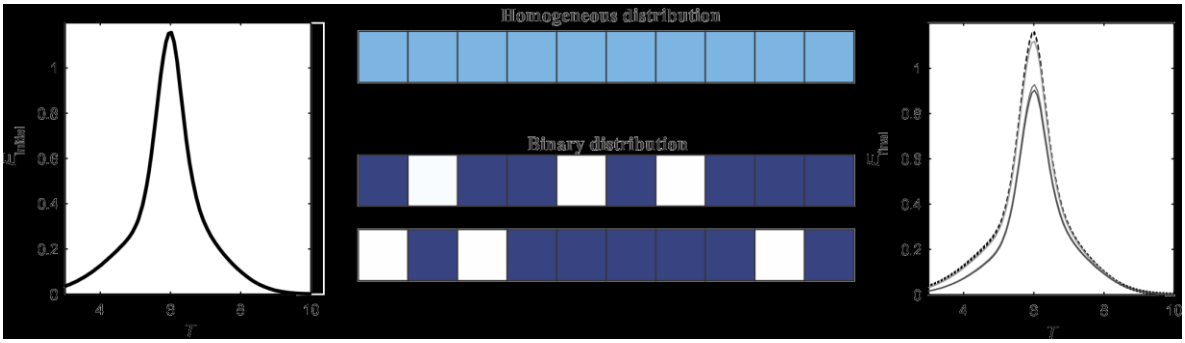

Figure 9. Schema of the two types of ice distributions for $f_i = 0.3$. The initial spectrum $E_{initial}$ (*left*) is advected along the ice transect. Depending on the ice distribution (*middle*), homogeneous (*top*, $f_i^* = f_i$ in all sub-cells) or binary (*bottom*, 3 sub-cells with $f_i^* = 1$ and 7 sub-cells with $f_i^* = 0$), the final spectrum E_{final} is different (*right*, full lines are the three final spectra, the dotted line is $E_{initial}$). Only 2 over 120 possible cases are represented for the binary distribution with $f_i = 0.3$ (Figure 10).

For a given concentration f_i, there are N possible binary transects (Figure 10), with

$$N = \binom{n_x}{n_i} = \frac{n_x!}{n_i!(n_x - n_i)!} \tag{2.13}$$

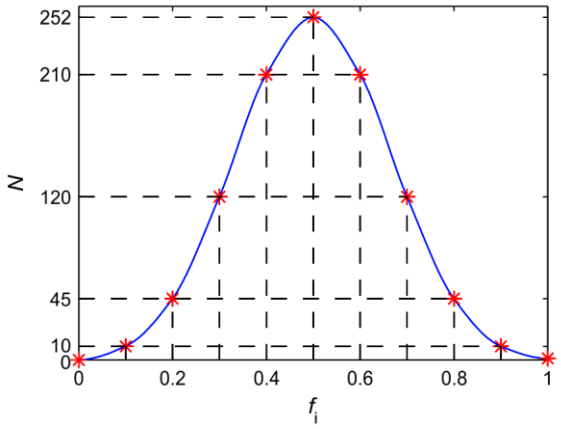

Figure 10. Number of binary transects (N) for each ice concentration (f_i).

The governing equation (1) solved by WIM is then simplified depending on f_i^*:

$$\frac{1}{c_g} D_t E(\omega, x, t) = \begin{cases} S_{in} + S_{wc} & \text{if } f_i^* = 0 \quad (2.14a) \\ S_{ice} & \text{if } f_i^* = 1 \quad (2.14b) \end{cases}$$

Several runs are made with ice concentration varying from 0 to 1 and wind speed from 0 to 30 m/s. The values of all the other parameters used are presented in Table 4. The incident JONSWAP spectrum (Hasselmann *et al.*, 1973) is expressed in terms of the peak frequency ω_p and the significant wave height H_s as :

$$E_i(\omega) = 0.2 H_s^2 \frac{\omega_p^4}{\omega^5} \exp\left[\frac{-5}{4}\left(\frac{\omega_p}{\omega}\right)^4\right] 3.3^{\exp\left[\frac{-(\omega-\omega_p)^2}{2\sigma^2\omega_p^2}\right]} \tag{2.15}$$

where σ is the spreading factor around the peak frequency :

$$\sigma = \begin{cases} 0.07 & \text{if } \omega < \omega_p \quad (2.16a) \\ 0.09 & \text{if } \omega > \omega_p \quad (2.16b) \end{cases}$$

Table 4. Fixed default parameters used for WIM.

Quantity	Symbol	Value
Grid cell size	ΔX	5 km
Subgrid cell size	Δx	500 m
Number of sub-cells	n_x	10
Ice thickness	h	0.5 m
Floes mean diameter	$\langle D \rangle$	200 m
Incident peak period	T_p	6 s
Incident peak frequency	f_p	$1/6$ Hz
Incident significant height	H_s	1 m
Minimum wave frequency	f_{min}	$1/20$ Hz
Maximum wave frequency	f_{max}	$1/2.5$ Hz
Number of frequency bins	n_w	61

2.2.5. Results and discussion

2.2.5.1. Competition between generation and attenuation processes

WIM is run in homogeneous ice transects to quantify the competition between open water and under-ice processes (Figure 11) in the usual way to model waves and ice interactions for a 5-km transect. Runs are performed with constant ice concentrations varying from 0 to 1 with an increment of 0.1 while the wind varies from 0 to 30 m s^{-1} with an increment of 2 m s^{-1}, for a total of 176 cases. Figure 11 shows the relative (i.e. normalized by the initial value) evolution of the total energy m_0 and peak energy E_p for an initial JONSWAP spectrum with T_p = 6 s and H_s = 1 m. It is interesting to focus on the equilibrium contour, i.e., the value of U_{10} and f_i for which no evolution occurs (line of ratio 1 in Figure 11). This contour highlights the conditions when the wave growth and wave attenuation balance each other. This curve is not exactly the same for m_0 and E_p because of the repartition of the energy over the spectrum; even if the peak energy is the same, the total energy can be different because the ice tends to reduce the high-frequencies energy whereas it does not affect much the low-frequencies. The figure shows also that the wind has little effect for ice concentrations above 0.6 on the total energy and above 0.8 for the peak energy, indicated by the fact that the contours become almost vertical above these

concentration values. Contours are vertical for wind speeds below U_{10} = 7.5 m s^{-1}, because the drag coefficient is constant for wind speeds below this value. The figure shows that for the initial spectrum used, the waves are not fully attenuated, even for f_i = 1, which is coherent with the first observations of Squire and Moore (1980) that longer waves can travel long distance inside the ice pack.

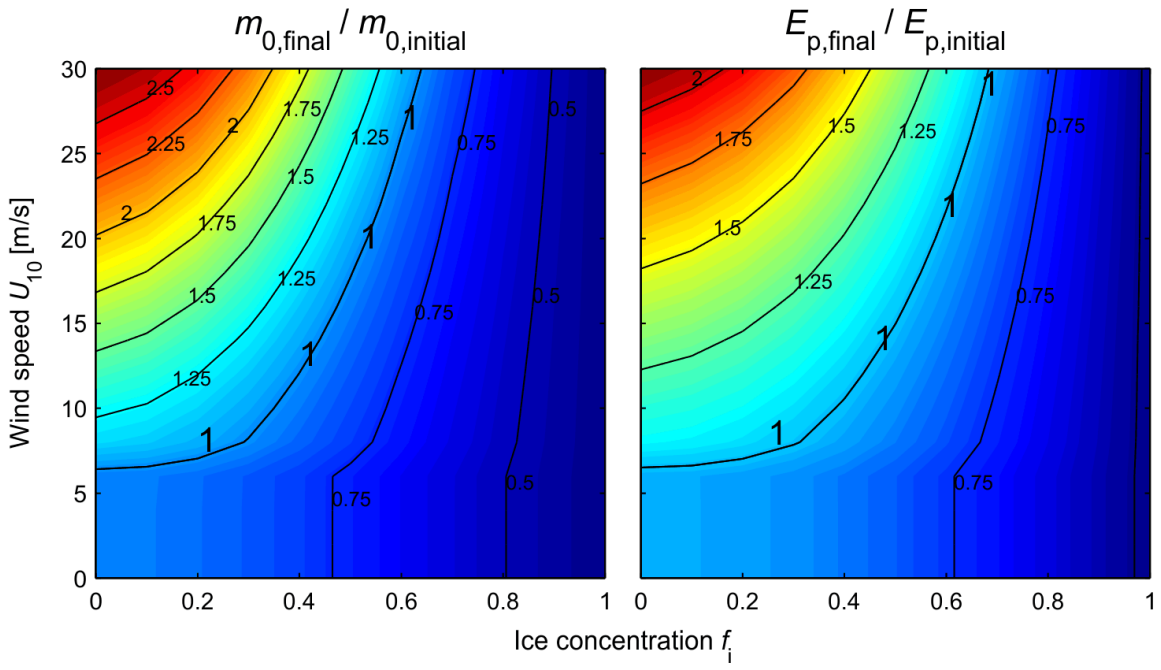

Figure 11. *Left* : evolution of total energy m_0 presented as the ratio between final and initial states for a 5-km transect with homogeneous ice concentration from 0 to 1 and constant and stationary wind from 0 to 30 m s^{-1}, for an initial JOSNWAP spectrum with T_p = 6 s and H_s = 1m. *Right* : same as left panel for the peak energy E_p.

These results are consistent with those of Perrie and Hu (1996), who noted that under certain ice and wind conditions, waves could be generated and grow inside a partially ice covered region, as firstly suggested by observations of Wadhams (1973). Masson and LeBlond (1989) investigated the same issue by asking 'Is there a minimum wind speed for which waves can still grow in the presence of a certain ice cover?', and found a minimum value for U_{10} of 13 m s^{-1} and 16 m s^{-1} for f_i = 0.1 and f_i = 0.2 respectively, whereas Figure 11 shows this value is closer to 6-8 m s^{-1} for the equilibrium contour. Nonetheless, the total energy is multiplied by 1.5 for U_{10} = 13 m s^{-1} and U_{10} = 17 m s^{-1} for f_i = 0.1 and

f_i = 0.2 respectively. Part of this difference probably comes from the initial spectrum used: Masson and LeBlond (1989) used a JONSWAP spectrum with T_p = 3.3 s, whereas a JONSWAP spectrum with T_p = 6 s is used here, so that more energy is carried by the longer waves, which are less attenuated by the ice. However, WIM was also run with the same spectrum as Masson and LeBlond (1989) and the minimum U_{10} value for energy growth is 8 m s^{-1} and 11 m s^{-1} for f_i = 0.1 and f_i = 0.2. A smaller peak period in the formulation of the spectrum leads to a more efficient attenuation, and the minimal wind needed to increase the total energy has to be stronger. The other part of the difference between the results of Masson and LeBlond (1989) and this study comes from the fact that they studied the directional evolution of the spectrum, and thus calculated the wave-wave interaction source term, which is neglected here. This term removes some energy of the peak period to redistribute it within the spectrum. Part of this energy is added to the shorter waves that experience more attenuation by the ice, so the overall evolution of the total energy is less important than when such a redistribution of the energy is neglected.

2.2.5.2. Sensitivity to the ice distribution

The results of Figure 11 are valid only if the ice concentration is constant for 5-km, which is an approximation of the ice behaviour at fine scale. It is more likely that the ice has a heterogeneous distribution inside the 5-km scale, so the evolution of the wave spectrum can be different. It is thus important to quantify the possible error associated with this approximation, or to confirm that it is valid. Binary distributions were chosen as a way to represent the ice distribution at a subgrid scale. This choice initially comes from the idea of representing each floe along an ice transect, to calculate the portion of wave energy reflected at each water-ice interface, and accurately differentiate the medium where the waves are propagating. This is obviously almost impossible to solve numerically because the spatial resolution should be as small as the smallest floe, or should vary depending on each floe size. Nevertheless, the idea of differentiating the propagation medium has remained by distributing the ice into completely ice covered sub-cells ($f_i^* = 1$) and open water ones ($f_i^* = 0$), which is the opposite of considering the ice is homogeneous. Another

motivation is that sea ice also tends to aggregate in bands or clusters of floes in the presence of wind and waves (Wadhams, 1973; Hermann, 2012). The most realistic way to distribute the ice at fine scale would probably be a partial non-constant ice concentration in each 500-m cell, so the total concentration inside the 5-km transect stays the same, but such a representation would give far too many cases to run. The choice of representing the ice by concentration bins of 1 or 0 is convenient in order to limit the number of cases for a given ice concentration (Figure 10). It also removes the question whether the ice or the wind acts first on the wave spectrum inside a partially ice-covered cell, which would be equivalent to choose between an explicit or an implicit scheme for the ice term.

The variability induced by the ice distribution is shown in Figure 12. For given U_{10} and f_i values, the corresponding N simulations are run and the final N spectra are compared. Figure 12 shows the relative standard deviation (the standard deviation normalized by the mean value) and the extreme deviation (difference between extrema normalized by the mean value) of m_0 and E_p for each U_{10} and f_i values (these values are the same as in Figure 11, for a total of 20 146 simulations). Those graphs show that the ice distribution has an effect on the final wave spectrum, with a maximum difference of 16% for m_0, and 9% for E_p. The relative standard deviation is less important, 4% and 2% at most for m_0 and E_p respectively. For all binary cases, the final maximum energy is always obtained when the ice occupies the first sub-cells of the transect, whereas the final energy is minimum when the ice is at the end of the transect. This figure also shows that the contours are asymmetric, and the sensitivity is higher for an ice concentration of 10% to 30%. This can be explained because at lower ice concentration, wave attenuation is weaker and the wind has a stronger effect on the wave spectrum, and leads to a higher variability depending on where the ice sub-cells are located within the transect. As ice concentration increases, more energy is removed and the variability decreases.

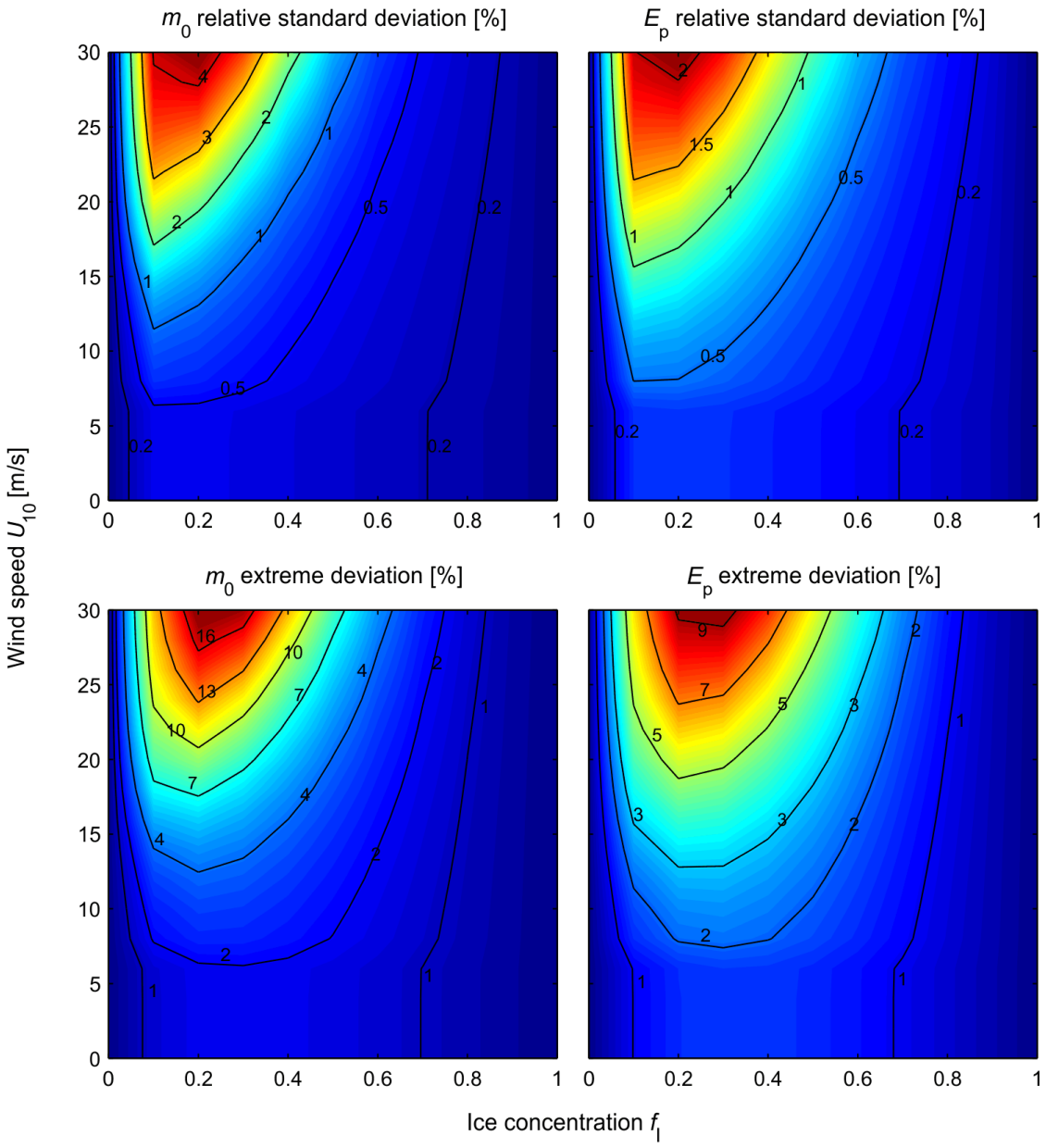

Figure 12. *Top* : relative standard deviation (standard deviation standardized by mean value) for m_0 (*left*) and E_p (*right*) at the end of the 5-km transect for all possible binary transects for ice concentrations between 0 and 1. *Bottom* : extreme deviation (difference between the maximum and minimum values standardized by the mean value) for m_0 (*left*) and E_p (*right*). Wind speed varies from 0 to 30 m s^{-1}.

Perrie and Hu (1996) studied the sensitivity of their model of waves propagating through an ice covered transect with generation by wind, and found that the most important

factors are ice concentration and floe size, whereas ice thickness and wind speed induce less variability. For homogenous transects, WIM is indeed weakly sensitive to the ice thickness for ice concentrations lower than 0.5, and slightly more sensitive for higher concentrations. For example, for an ice thickness of 2 m, the wind needs to be 12% to 20% (1 to 7-8 m s^{-1}) stronger to compensate wave attenuation for concentrations between 0.1 and 0.5, compared to the thickness used here (0.5 m). This means the equilibrium contour in Figure 11 would be slightly more abrupt for a thicker ice. Also, the incident spectrum is fully attenuated for $f_i = 0.8$ with an ice thickness of 2 m on a 5-km transect. However, the standard and extreme deviations differ by 2.5% and 6% respectively when using a maximum floe size from 50 and 500 meters with the binary distribution, which is less than half the variability induced by the ice distribution. This shows that the way ice is distributed at fine scale is an even more important factor of variability for our model than the ones Perrie and Hu (1996) considered the most important. In WIM, the attenuation comes from the partial reflection of the wave energy on a change of propagation medium, whereas Perrie and Hu (1996) studied the energy transferred from waves to floes making them roll, pitch or heave. Reducing the floe mean diameter implies a larger number of water-ice interfaces in WIM, whereas it gives a greater transfer of energy in Perrie and Hu's (1996) model. The effective loss of energy from the waves appears to be more sensitive to the floe size when considering energy transfer from waves to floes than energy reflection.

2.2.5.3. Source of the variability

To better understand the source of the variability, one particular case was chosen to take a closer look at the evolution of the wave spectrum and the source term in each cell (Figure 13). This case is the one with $f_i = 0.3$ and $U_{10} = 25$ m s^{-1}, for which the extreme deviation is 12% for the total energy and 7% for the peak energy as it can be seen on Figure 12. For this particular case, the three ice distributions are shown in Figure 13 (top panel); the homogeneous case in green and the two binary distributions that lead to the extreme final spectra (red and blue for maximum and minimum respectively). As

mentioned earlier, the final energy is maximum if the ice is distributed on the first sub-cells of the transect, whereas it is minimum if the ice occupies the last sub-cells, regardless to the concentration. The middle panel of Figure 13 shows the evolution of the total energy $m_{0,i}$ in each sub-cell i (normalized by its initial value $m_{0,initial}$), and the two bottom panels show the wave spectrum E and the total source term S in each cell.

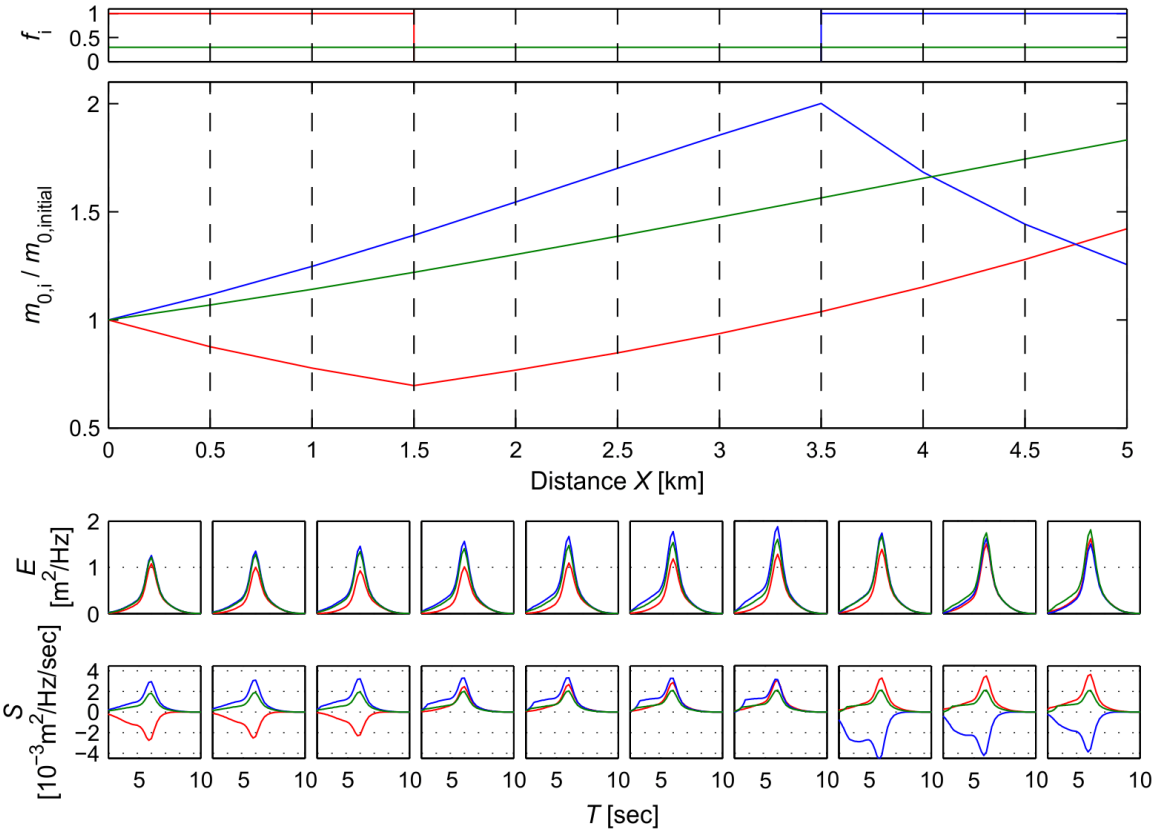

Figure 13. Evolution of the waves along a 5-km transect with 3 ice distributions, for a total concentration of 0.3 with a 25 m s^{-1} wind speed. The first panel shows the three different ice transects (homogeneous case in green, the red and blue cases are the binary distributions that lead to the final maximum and minimum energy respectively). The second panel shows the evolution in each sub-cell of m_0 (normalized by its initial value), and the two last panels show respectively the wave spectrum and the source term in each sub-cell.

For the homogeneous distribution (green), the source term does not vary a lot because the three source terms are almost linear, so as the waves grow, the wind generates more waves, but the ice and the white capping dissipate more energy, and the growth rate is

almost constant and is dominated by the wind generation for this value of ice concentration. This is not the same for the binary cases because the open water and ice processes do not affect the wave spectrum simultaneously; if the ice concentration is 1 in the sub-cell, only the attenuation by ice is effective, whereas in a 0 concentration sub-cell, only the wind and white capping affect the spectrum. For the red case, the ice attenuates the initial spectrum in the three first sub-cells, with a lesser effect from sub-cell to sub-cell as the waves are attenuated. So when the waves reach the open water, the spectrum on which the wind acts has less energy and the wave growth is weaker than for the blue case. For this case, the wind directly acts on the initial spectrum for the seven first sub-cells of open water with the highest growth rate of the three cases, but when the waves encounter the ice, the attenuation is much stronger because of the greater energy, and leads to the minimal energy at the end. It is important to point out that this particular case leads to a higher final energy with the homogeneous ice distribution than for all possible binary combinations, but with ice concentrations above 0.5, the average final energy for all the binary combinations is higher than the final energy obtained with the homogeneous distribution, no matter the wind speed.

2.2.5.4. Illustration of the variability for an idealised case

To illustrate how much the ice distribution can influence the waves modelled by WIM, it has been run on a 75-km long transect, with the ice concentrations given at 5-km scale, representing an ice band perpendicular to the wave direction with a 25 m s^{-1} wind blowing in the same direction. The ice concentration increases from 0.1 to 0.8 in the first eight 5-km cells, and then decreases again to 0.1, with 0.1 concentration steps. For the three cases (Figure 14, top panels), the ice concentration is the same in each 5-km cells, but distributed in three different ways in the ten 500-m sub-cells.

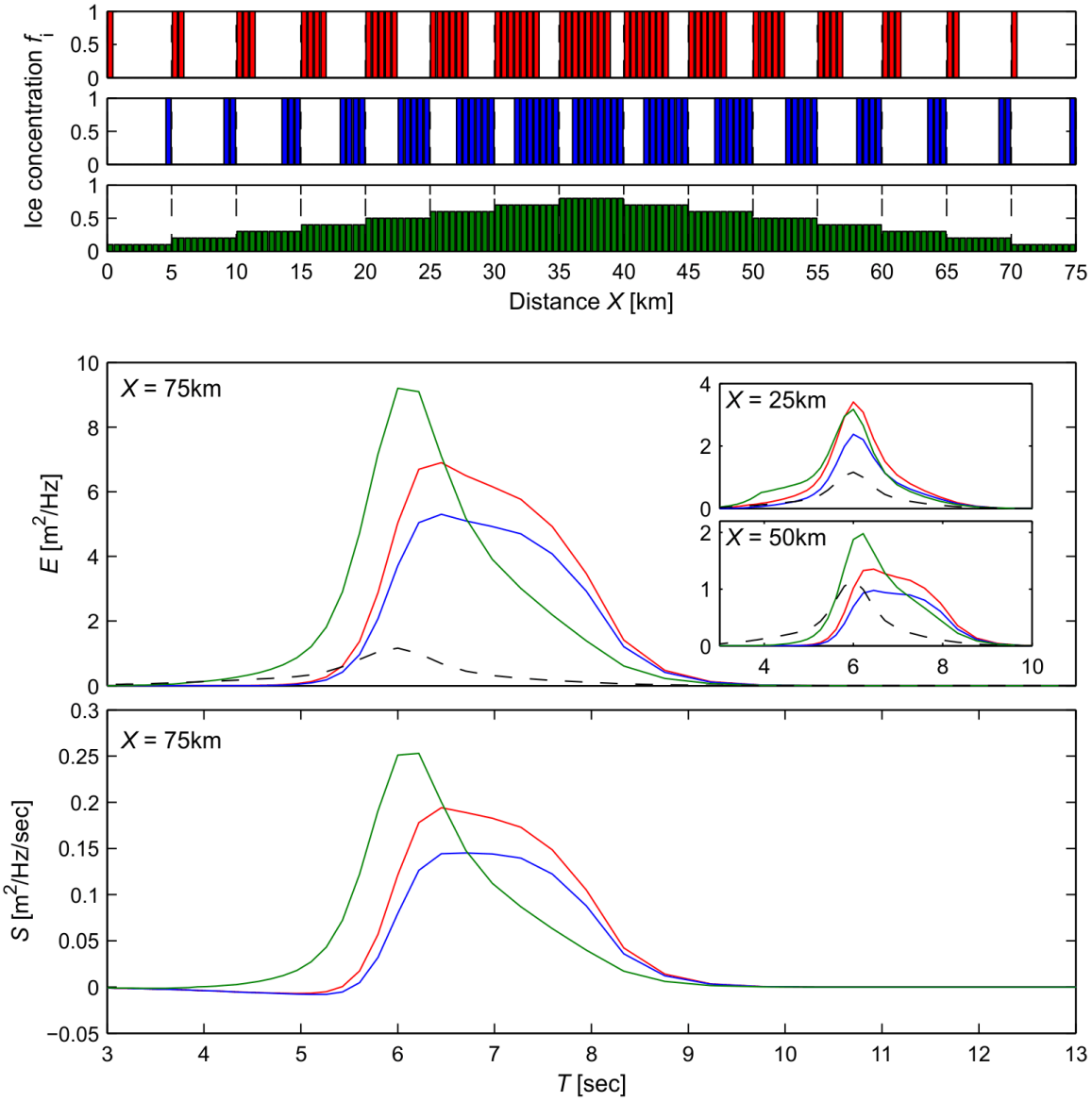

Figure 14. Evolution of wave energy along an idealised 75-km transect. The ice concentration is given at 5-km spatial resolution, and is distributed in three different ways at 500-m resolution (three top panels) with the same colors as in Figure 13. The middle panel shows the final wave spectrum for each case (the dashed black line is the initial spectrum), and the two sub-panels show respectively the wave spectrum at 25 km and 50 km for each case. The bottom panel shows the sum of all the source terms for each case.

For the first case (red), the ice has a binary distribution, and is located at the beginning of the 5-km cell. This distribution gives the maximum wave energy within 5-km cell (see section 2.2.5.3). The second case (blue) is the opposite; the ice is at the end of each

5-km cell, which is the distribution that gives the minimum wave energy. The third case (green) has an homogeneous distribution at 5-km scale. For each case, the final spectrum and the total of the source term is represented in the middle and bottom panel respectively. The spectra for two intermediate distances are presented in the sub-panels of the middle panel. They show the three spectra at 25 km (top) and 50 km (bottom), i.e. before reaching the region where $f_i > 0.5$ and before leaving this very same region.

These graphs show that the ice distribution has an effect not only on the total energy but also on the shape of the final spectrum. The total energy is 35% and 17% higher for the homogeneous case than for the minimum and maximum binary cases respectively, and the total energy differs by 22% between those two cases. For the homogeneous case, the energy for the short waves is more important and the peak period is almost the same as the initial state. The shape of the spectrum obtained with a binary distribution is different from the homogeneous case, the spectrum being less sharp and the peak period being moved to the lower frequencies. As the long waves need a longer fetch to be generated, it is not surprising that the binary distribution allows the energy of such waves to increase, while the fact that there is some ice in every cell for the homogeneous case prevents their formation. For the high frequency tail of the spectrum, the energy is close to zero for the binary cases because the totally ice-covered sub-cells have removed all this energy by attenuating the shorter waves as indicated by the negative source term for waves with 4 to 5.5 seconds periods.

2.2.6. Summary and conclusions

WIM is a simple model that initially simulated how waves are attenuated when propagating through an ice transect. Here we enhanced this model by implementing the wind generation and white-capping dissipation source terms. This provided a simple tool to study the evolution of a wave spectrum travelling in partially ice-covered seas, in order to better understand the coupled interaction between atmosphere, ocean and sea ice. The

results show that under particular circumstances, waves can be generated and grow inside an ice region, which is consistent with the first observations of Wadhams (1983) and the results of other studies (Masson and LeBlond, 1989; Perrie and Hu, 1996). The wind action is strongly dependant on how ice is distributed at a subgrid scale, with differences up to 15% in the final amount of wave energy in the spectrum. The shape of the spectrum is also affected by the ice distribution at fine resolution, the energy being more important for low-frequency waves for binary concentrations than for homogeneous concentrations. Despite the quantitative differences about the amount of energy involved, the wind has an effect on waves inside a dispersed ice field, and cannot be neglected when studying the waves and ice interactions, especially in a context of climate change that will probably lead to sparser and sparser ice fields, in the GSL or other ice covered seas. Further simulations should take this into account, by including the waves attenuation by ice in the physics of the actual wave models.

In this perspective, the issue with these models to reduce the spatial resolution was explored with WIM, by focusing on the sensitivity of the model to the ice distribution at fine scale. This was made by running the model along binary ice transects and homogeneous ones for the same value of ice concentration. The comparison of these several runs highlighted the variability of the final modelled spectrum, which is even more important that the variability induced by other parameters that were previously believed to be the most important ones, like the ice thickness or the floe diameter. The ice distribution at fine scale is thus an important factor when coupling wind generation and ice attenuation.

Without proposing a new parameterization of the ice distribution, this study provides insights on the uncertainties and sensitivities of future coarse-resolution coupled wave-ice models, especially in coastal areas where spatial resolution needs to be as fine as the bathymetry requires.

2.2.7. Acknowledgments

This project was funded by the government of Québec (Ministère des Transports du Québec) and is a contribution to the research program of Québec-Océan. We are very grateful to Timothy Williams for sharing the WIM source code.

CONCLUSION

Ce projet de maîtrise a permis d'une part de fournir une amélioration de l'évaluation du climat de vagues hivernal dans l'EGSL par le développement d'une nouvelle méthode de prise en compte de la glace pour la caractérisation du climat de vagues à long-terme. D'autre part, l'étude de sensibilité du modèle WIM amélioré avec l'implémentation des processus d'eau libre est une étape de plus de franchie vers la considération de l'atténuation des vagues par la glace dans les modèles couplés vagues-glace, lesquels deviendront un outil précieux pour une prévision précise des conditions océaniques dès lors qu'ils seront inclus dans les systèmes opérationnels.

La méthode empirique de prise en compte de la glace est intéressante par sa simplicité. Elle ne nécessite en effet que les données de température de l'air à 2 m de la surface pour estimer les caractéristiques moyennes du couvert de glace de l'EGSL. Son intérêt réside principalement dans sa grande rapidité d'exécution et, conséquemment, qu'un grand nombre de simulations climatiques peut être utilisé pour construire une projection d'ensemble et ainsi quantifier la variabilité intrinsèque du système. Les résultats obtenus indiquent que la durée du couvert de glace pour la période 2071-2100 sera environ deux fois plus courte que pour la période du passé récent de 1981-2010. De plus, la concentration maximale du couvert de glace de l'EGSL sera aussi deux fois moins grande en moyenne pour la période future que pour le passé récent. Cette réduction à la fois spatiale et temporelle du couvert de glace aura un effet cumulé sur le climat de vagues, représentant une atténuation moins efficace d'environ 80% par rapport au passé récent. Sachant que les tempêtes dans l'EGSL surviennent préférentiellement tard à l'automne et en hiver, la disparition de la banquise pourrait se traduire par des événements d'érosion côtière de plus

en plus importants. La tempête du 6 décembre 2010 qui a frappé l'estuaire maritime en est un bon exemple. Ces résultats doivent néanmoins être interprétés avec précaution. Une simulation climatique ne représente qu'une réalisation possible de l'évolution de climat, et seulement la considération d'un grand nombre d'entre elles permet d'établir une probabilité d'occurrence fiable. Ainsi, l'utilisation de seulement huit simulations pour l'évolution du couvert de glace parait faible. L'utilisation d'un plus grand nombre de simulations serait donc préférable pour augmenter la fiabilité des résultats, d'autant plus que ces huit simulations suivent toutes le scénario climatique A2 du Groupe d'experts intergouvernemental sur l'évolution du climat (GIEC) produit en 2007. L'utilisation de simulations basées sur les scénarios proposées par le cinquième rapport du GIEC (Stocker *et al.*, 2013) est recommandée pour mettre à jour ces résultats. De plus, les relations empiriques établies entre degré-jours de gel et couvert de glace ne tiennent pas compte des deux derniers hivers (2012-2013 et 2013-2014), qui permettraient de mieux caractériser le couvert de glace en consolidant ces relations empiriques.

Finalement, l'atténuation des vagues est aussi déterminée de manière empirique et ne tient pas compte des interactions complexes entre vagues et glace. En réalité, l'atténuation dépend à la fois des caractéristiques des vagues (période) et de la glace (épaisseur, morphologie, taille des floes). Ainsi, la méthode proposée est une simplification de la réalité, mais représente tout de même un raffinement par rapport aux estimations traditionnelles de considérer une absence complète de vagues en hiver, ou de considérer que les vagues peuvent être simulées comme si aucune glace n'était présente. Ruest (2013) montre néanmoins que la dernière approximation est valide pour quiconque voudrait estimer les extrêmes du climat de vague pour la période 2071-2100.

La gestion des risques en milieu côtier ne repose pas seulement sur notre capacité à projeter le climat dans le futur, mais aussi sur notre capacité à prévoir l'état de la mer sur des horizons beaucoup plus courts (heures, jours, semaines). Dans ce dernier cas, l'outil de prédilection est la modélisation numérique des processus atmosphériques et océaniques couplés. Néanmoins, les modèles actuellement en opération au Canada et même dans le

monde n'incluent pas les interactions vagues-glace, ou, s'ils le font, de manière très idéalisée. Dans une optique de perfectionnement de ces modèles, l'étude menée avec la version de WIM améliorée, comprenant les processus de génération en eau libre, a mis en évidence l'importance de bien représenter la répartition spatiale de la glace afin de bien simuler le spectre de vagues. Les simulations montrent effectivement que le spectre de vagues peut gagner de l'énergie si la concentration de glace est inférieure à 50%, dépendamment du vent. Ces résultats indiquent aussi que l'énergie des vagues ne peut être qu'atténuée pour des concentrations supérieures à 60% pour les conditions de vagues représentatives des conditions de l'EGSL. Cette valeur appuie le choix, réalisé arbitrairement dans le premier chapitre, pour la valeur limite de concentration de glace au-delà de laquelle les vagues sont considérées totalement atténuées. En effet, pour des vents de 20 m s^{-1}, la Figure 11 montre que l'énergie totale est atténuée de 25% en 5 km, et donc qu'il faut moins de 40 km pour que l'énergie soit atténuée d'un facteur 10 dans de telles conditions. La Figure 1 montre que pour 60% de glace, la majorité du trait de côte du St-Laurent est protégé par une telle distance de glace ; il parait donc légitime de considérer que les vagues sont complètement atténuées à l'échelle du golfe au-delà d'une concentration de 60%. L'étude du chapitre II démontre par ailleurs l'importance de la distribution spatiale de la glace à fine échelle, contrairement à l'hypothèse faite dans le chapitre I où les vagues sont atténuées de manière égale sur toute la région, sans tenir compte de la répartition de la glace. En effet, sur une distance de 5 km, pour une concentration de glace donnée, sa distribution engendre des différences de plus de 15% sur l'énergie totale du spectre de vagues, et d'environ 10% sur l'énergie modale. Cette considération est donc à prendre en compte pour l'implémentation des interactions vagues-glace dans des modèles de vagues couplés, particulièrement dans une optique d'en améliorer la résolution spatiale, au même titre que les forçages atmosphériques ou la bathymétrie. Ces résultats suggèrent également que les processus affectant la distribution spatiale de la glace, auxquels les vagues contribuent notamment, mériteront d'être étudiés plus en détail.

RÉFÉRENCES BIBLIOGRAPHIQUES

Anandhi, A., Frei, A., Pierson, D.C., Schneiderman, E.M., Zion, M.S., Lounsbury, D., Matonse, A.H. (2011). Examination of change factor methodologies for climate change impact assessment. *Water Resources Research*, 47(3): W03501, 10 p.

Assel, R.A. (1980). Maximum freezing degree-days as a winter severity index for the great lakes, 1897-1977. *Monthly Weather Review*, 108: 1440-1445.

Bennetts, L.G., Squire, V.A. (2012). On the calculation of an attenuation coefficient for transects of ice-covered ocean. *Proceedings of the Royal Society A-mathematical physical and engineering sciences*, 468: 136-162.

Bennetts, L.G., Peter, M.A., Squire, V.A., Meylan, M.H. (2010). A three-dimensional model of wave attenuation in the marginal ice zone. *Journal of Geophysical Research*, 115: C12043, 12 p.

Bernatchez, P., Dubois, J.M.M. (2004). Bilan des connaissances de la dynamique de l'érosion des côtes du Québec maritime laurentien. *Géographie physique et Quaternaire*, 58(1): 45-71.

Booij, N., Ris, R.C., Holthuijsen, L.H. (1999). A third-generation wave model for coastal regions, Part 1: Model description and validation. *Journal of Geophysical Research*, 104(C4): 7649-7666.

Bouws, E., Komen, G.J. (1983). On the balance between growth and dissipation in an extreme, depth-limited wind-sea in the southern North Sea. *Journal of Physical Oceanography*, 13(9): 1653-1658.

Côté, J., Gravel, S., Méthot, A., Patoine, A., Roch, M., Staniforth, A. (1998). The operational CMC-MRB global environmental multiscale (GEM) model. Part I: Design considerations and formulation. *Monthly Weather Review*, 126(6): 1373-1395.

De Carolis, G., Olla, P., Pignagnoli, L. (2005). Effective viscosity of grease ice in linearized gravity waves. *Journal of Fluid Mechanics*, 535: 396-381.

Dumont, D., Kohout, A., Bertino, L. (2011). A wave-based model for the marginal ice zone including a floe breaking parameterization. *Journal of Geophysical Research*, 116: C04001, 12 p.

Fequet, D. (2002). *MANICE: Manual of Standard Procedures for Observing and Reporting Ice Conditions*, 9th ed., Canadian Ice Service, Environment Canada, Ottawa, 226 p.

Forbes, D.L., Parkes, G.S., Manson, G.K., Ketch, L.A. (2004). Storms and shoreline retreat in the southern Gulf of St. Lawrence. *Marine Geology*, 210(1): 169-204.

Galbraith, P.S. (2006). Winter water masses in the Gulf of St. Lawrence. *Journal of Geophysical Research*, 111: C06022, 23 p.

Galbraith, P.S., Chassé, J., Larouche, P., Gilbert, D., Brickman, D., Pettigrew, B., Devine, L., Lafleur, C. (2013). *Physical Oceanographic Conditions in the Gulf of St. Lawrence in 2012*. Technical report, DFO Canadian Science Advisory Secretariat Research Document 2013/026, 77 p.

Günther, H., Hasselmann, S., Janssen, P.A.E.M. (1992). *The WAM Model Cycle 4 (Revised Version)*. Technical Report No. 4, Deutsches Klimatisches Rechenzentrum, Hamburg, 17 p.

Hasselmann, K., Barnett, T.P., Bouws, E., Carlson, H., Cartwright, D.E., *et al.* (1973). Measurements of wind-wave growth and swell decay during the Joint North Sea Wave Project (JONSWAP). *Deutsche Hydrographische Zeitschrift*, Ergänzungsheft A12, 95 p.

Hasselmann, K. (1974). On the spectral dissipation of ocean waves due to white capping. *Boundary-Layer Meteorol.*, 6(1-2): 107-127.

Herman, A. (2012). Influence of ice concentration and floe-size distribution on cluster formation in sea-ice floes. *Central European Journal of Physics*, 10(3): 715-722.

Hill, B.T., Ruffman, A., Drinkwater, K., (2002). Historical record of the incidence of sea ice on the scotia shelf and the Gulf of St. Lawrence. *Ice in the Environment: Proceedings of the 16th International Symposium on Ice*, International Association of Hydraulic Engineering and Research, v. 1, 313-320.

Holthuijsen, L.H. (2007). *Waves in oceanic and coastal waters*. Cambridge University Press, 387 p.

Janssen, P.A.E.M. (1991). Quasi-linear theory of wind-wave generation applied to wave forecasting. *Journal of Physical Oceanography*, 21(11): 1631-1642.

Johnston, D.W., Friedlaender, A.S., Torres, L.G., Lavigne, D.M. (2005). Variation in sea ice cover on the east coast of Canada from 1969 to 2002: climate variability and implications for harp and hooded seals. *Climate Research*, 29(3): 209–222.

Keller, J.B. (1998). Gravity waves on ice-covered water. *Journal of Geophysical Research*, 103(C4): 7663-7669.

Kohout, A.L., Meylan, M.H. (2006). A model for wave scattering in the marginal ice zone based on a two-dimensional floating-elastic-plate solution. *Annals of Glaciology*, 44: 101-107.

Kohout, A.L., Meylan, M.H. (2008). An elastic plate model for wave attenuation and ice floe breaking in the marginal ice zone. *Journal of Geophysical Research*, 113: C09016, 17 p.

Kohout, A.L., Meylan, M.H., Plew, D.R. (2011). Wave attenuation in a marginal ice zone due to the bottom roughness of ice floes. *Annals of Glaciology*, 52: 118-122.

Kohout, A.L., Williams, M.J.M., Dean, S.M., Meylan, M.H. (2014). Storm-induced sea-ice breakup and the implications for ice extent. *Nature*, 509(7502): 604-607.

Komen, G.J., Hasselmann, K., Hasselmann, K. (1984). On the existence of a fully developed wind-sea spectrum. *Journal of Physical Oceanography*, 14(8): 1271-1285.

Langhorne, P.J., Squire, V.A., Fox, C., Haskell, T.G. (1998). Break-up of sea ice by ocean waves. *Annals of Glaciology*, 27: 438-442.

Lebedev, V.V. (1938). Rost l'da v arkticheskikh rekakh i moriakh v zavisimosti ot otritsatel'nykh temperatur vozdukha. *Problemy Arktiki*, 5: 9-25.

Lee, O.S., Simpson, L.S. (1954). *A practical method of predicting sea ice formation and growth.* Tech. Rep. 4. Hydrographic office, Washington. 27 p.

Liu, A.K., Mollo-Christensen, E. (1988). Wave propagation in a solid ice pack. *Journal of Physical Oceanography*, 18: 1702-1712.

Masson, D., LeBlond, P.H. (1989). Spectral evolution of wind-generated surface gravity waves in a dispersed ice field. *Journal of Fluid Mechanics*, 202: 43-81.

Nakicenovic, N., Alcamo, J., Davis, G., De Vries, B., Fenhann, J., Gaffin, S., *et al.* (2000). *IPCC special report on emissions scenarios: a special report of Working Group III of the IPCC*. Cambridge University Press, Cambridge, UK, 599 p.

Neumeier, U., Ruest, B., Lambert, A., Bismuth, E., Dumont, D., Jacob, D., Savard, J.-P., Joly, S. (2013). *Modélisation du régime des vagues du golfe et de l'estuaire du Saint-Laurent pour l'adaptation des infrastructures côtières aux changements climatiques*. Rapport présenté au ministère des Transports du Québec. Institut des sciences de la mer de Rimouski, Université du Québec à Rimouski, 284 p.

Newyear, K., Martin, S. (1999). Comparison of laboratory data with a viscous two-layer model of wave propagation in grease ice, *Journal of Geophysical Research*, 104(C4): 7837-7840.

Ouellet, Y., Drouin, A. (1991). Définition des conditions de vagues pour la conception d'un havre de pêche à Sept-îles. *Canadian Journal of Civil Engineering*, 18(5): 851-863.

Overeem, I., Anderson, R.S., Wobus, C.W., Clow, G.D., Urban, F.E., Matell, N. (2011). Sea ice loss enhances wave action at the Arctic coast. *Geophysical Research Letters*, 38: L17503, 6p.

Perrie, W., Hu, Y. (1996). Air-ice-ocean momentum exchange. Part I: Energy transfer between waves and ice floes. *American Meteorological Society*, 26: 1705-1720.

Phillips, O.M. (1957). On the generation of waves by turbulent wind. *Journal of Fluid Mechanics*, 2(5): 417-445.

Pierson, W.J., Moskowitz, L. (1964). A proposed spectral form for fully developed wind seas based on the similarity theory of SA Kitaigorodskii. *Journal of Geophysical Research*, 69(24): 5181-5190.

Rienecker, M.M., Suarez, M.J., Gelaro, R., Todling, R., Bacmeister, J., Liu, *et al.* (2011). MERRA: NASA's modern-era retrospective analysis for research and applications. *Journal of Climate*, 24(14): 3624-3648.

Richards, T.L. (1964). The meteorological aspects of ice cover on the great lakes. *Monthly Weather Review*, 92: 297-302.

Rodhe, B. (1952). On the relation between air temperature and ice formation in the Baltic. *Geografiska annaler*, 34: 175-202.

Roland, A., Ardhuin, F. (2014). On the developments of spectral wave models: numerics and parameterizations for the coastal ocean. *Ocean Dynamics*, 64(6): 833-846.

Ruest, B. (2014). *Utilisation d'un modèle paramétrique pour l'évaluation du climat de vagues de l'estuaire et du golfe du Saint-Laurent et son évolution future dans un contexte de changements climatiques*. Mémoire de maîtrise présenté à l'Université du Québec à Rimouski, Institut des Sciences de la Mer à Rimouski, Québec, Canada, 120 p.

Saucier, F.J., Roy, F., Gilbert, D., Pellerin, P., Ritchie, H. (2003). Modeling the formation and circulation processes of water masses and sea ice in the Gulf of St. Lawrence, Canada. *Journal of Geophysical Research,* 108(C8), 20 p.

Savard, J.-P., Bernatchez, P., Morneau, F., Saucier, F. (2009). Vulnérabilité des communautés côtières de l'est du Québec aux impacts des changements climatiques. *La Houille Blanche*, (2): 59-66.

Senneville, S., St-Onge Drouin, S., Dumont, D., Bihan-Poudec, A.-C., Belemaalem, Z., *et al.* (2013). *Modélisation des glaces dans l'estuaire et le golfe du Saint-Laurent dans la perspective des changements climatiques*. Rapport présenté au ministère des Transports du Québec, 384 p.

Smith, G.C., Roy, F., Brasnett, B. (2013). Evaluation of an operational ice–ocean analysis and forecasting system for the Gulf of St Lawrence. *Quarterly Journal of the Royal Meteorological Society*, 139(671): 419-433.

Snyder, R.L., Dobson, F.W., Elliott, J.A., Long, R.B. (1981). Array measurements of atmospheric pressure fluctuations above surface gravity waves. *Journal of Fluid Mechanics*, 102: 1-59.

Squire, V.A. (1993). The breakup of shore fast sea ice. *Cold Regions Science and Technology*, 21: 211-218.

Squire, V.A. (2007). Of ocean waves and sea-ice revisited. *Cold Regions Science and Technology*, 49: 110-133.

Squire, V.A., Moore, S.C. (1980). Direct measurement of the attenuation of ocean waves by pack ice. *Nature,* 283: 365-368.

Squire, V.A., Dugan, J.P., Wadhams, P., Rottier, P.J., Liu, A.K. (1995). Of ocean waves and sea ice. *Annual Review of Fluid Mechanics*, 27(1): 115-168.

Squire, V.A., Vaughan, G.L., Bennetts, L.G. (2009). Ocean surface wave evolvement in the Arctic Basin. *Geophysical Research Letters*, 36: L22502, 5 p.

Steele, M. (1992). Sea ice melting and floe geometry in a simple ice-ocean model. *Journal of Geophysical Research: Oceans (1978–2012)*, 97(C11): 17729-17738.

Steele, M., Morison, J.H., Untersteiner, N. (1989). The partition of air-ice-ocean momentum exchange as a function of ice concentration, floe size, and draft. *Journal of Geophysical Research: Oceans (1978–2012)*, 94(C9): 12739-12750.

Stocker, T.F., Qin, D., Plattner, G.K., Tignor, M., Allen, S.K., Boschung, J., Midgley, P.M. (2013). *Climate change 2013: The physical science basis*. Intergovernmental Panel on Climate Change, Working Group I Contribution to the IPCC Fifth Assessment Report (AR5) (Cambridge University Press, New York), 1526 p.

Thomson, J., Rogers, W.E. (2014). Swell and sea in the emerging Arctic Ocean. *Geophysical Research Letters*, 41: 3136-3140.

Timco, G.W., O'Brien, S. (1994). Flexural strength equation for sea ice. *Cold Regions Science and Technology*, 22(3): 285-298.

Tolman, H.L. (2003). Treatment of unresolved islands and ice in wind wave models. *Ocean Modelling*, 5(3): 219–231.

Tolman, H., Accensi, M., Alves, H., Ardhuin, F., Bidlot, J., *et al.* (2014). User manual and system documentation of WAVEWATCH III TM version 4.18. *Technical note, MMAB Contribution N.316*, 282 p.

Tuomi, L., Kahma, K.K., Pettersson, H. (2011). Wave hindcast statistic in the seasonally ice-covered Baltic Sea. *Boreal Environment Research*, 16: 451-472.

Vaughan, G.L., Squire, V. A. (2011). Wave induced fracture probabilities for Arctic sea-ice. *Cold Regions Science and Technology*, 67(1): 31-36.

Wadhams, P. (1973). Attenuation of swell by sea ice. *Journal of Geophysical Research*, *78*(18): 3552-3563.

Wadhams, P. (1983). A mechanism for the formation of ice edge bands. *Journal of Geophysical Research*, 88(C5): 2813-2818.

WAMDI Group (1988). The WAM model-a third generation ocean wave prediction model. *Journal of Physical Oceanography*, 18(12): 1775-1810.

Wang, R., Shen, H.H. (2010). Gravity waves propagating into an ice-covered ocean: a viscoelastic model. *Journal of Geophysical Research*, 115: C06024, 12 p.

Williams, T.D., Bennetts, L.G., Squire, V.A., Dumont, D., Bertino, L. (2013a). Wave–ice interactions in the marginal ice zone. Part 1: Theoretical foundations. *Ocean Modelling*, 71: 81-91.

Williams, T.D., Bennetts, L.G., Squire, V.A., Dumont, D., Bertino, L. (2013b). Wave–ice interactions in the marginal ice zone. Part 2: Numerical implementation and sensitivity studies along 1D transects of the ocean surface. *Ocean Modelling*, 71: 92-101.

Wu, J. (1982). Wind-stress coefficients over sea surface from breeze to hurricane. *Journal of Geophysical Research: Oceans (1978–2012)*, 87(C12): 9704-9706.

ANNEXE

CODE SOURCE DU MODÈLE WIM

Les lignes ci-dessous présentent le code source MATLAB (version R2012a) du modèle WIM (*wim_final*), ainsi que les sous-routines associées. La sous-routine d'advection de l'énergie des vagues (*advection*) provient de la version initiale de WIM (Williams *et al.*, 2013a), tout comme celle d'atténuation de l'énergie des vagues par la glace (*ice_att*). La génération par le vent (*wind_gen*), le white-capping (*white_cap*) et le limiteur d'évolution de l'énergie (*action_density_limiter*) ont été écrites en reprenant la formulation mathématique de chacun de ces termes tels que décrits par Holthuijsen (2007).

```
function [T,cice,Hsig,Ei,E,S_win,S_wcp,S_ice] = wim_final(C,h,D,U10,Tm,Hs)
%WIM_FINAL models the attenuation of waves propagating in an ice transect
%
% INPUTS
%   C     = ice concentration. For an homogeneous concentration, C is scalar in
% tenths. Otherwise, C is a vector of the size of the spatial grid, in
% fraction of 1 (0 < C < 1). In this version of WIM, if C is homogeneous,
% the transect is 5km long with spatial resolution of 500m.
%   h     = ice thickness in meters. h is a scalar.
%   D     = floes average diameter in meters. D is a scalar.
%   U10   = wind speed at 10m elevation in m/sec. U10 is a scalar.
%   Tm    = waves mean period to build the spectrum, in seconds. Tm is a scalar.
%   Hs    = waves significant height, in meters. Hs is a scalar.
%
% OUTPUTS
%   T     = waves periods in seconds. T is a vector the size of the frequency
        range.
%   cice  = ice concentration vector in fraction of 1. cice has the size of the
        spatial grid.
% If C is a vector, then cice = C.
%   Hsig  = final wave heigh in each cell in meters. Hsig has the size of the
        spatial
% grid.
%   Ei    = initial spectrum in m²/Hz.
%   E     = final wave spectrum in each cell [m²/Hz].
%   S_win = final wind source term in each cell in m²/Hz/sec.
%   S_wcp = final white-capping source term in each cell in m²/Hz/sec.
%   S_ice = final ice source term in each cell in m²/Hz/sec.

g = 9.81; % gravitational acceleration
dx = 500; % spatial resolution
% Ice conditions
```

```
if length(C) == 1    % Homogeneous ice concentration case
    nx   = 10;                    % 10 cells of 500m -> 5km long transect
    cice = zeros(1,nx)+C/10;      % homogeneous ice concentration vector
    hice = zeros(1,nx)+h;         % homogeneous ice thickness vector
    Dmax = zeros(1,nx)+D;         % homogeneous floe diameter vector
else                  % Variable ice concentration case
    nx            = length(C);    % number of cells
    cice          = C;            % ice concentration vector
    hice          = zeros(1,nx); % ice thickness vector size allocation
    hice(find(C)) = h;            % ice thickness vector
    Dmax          = zeros(1,nx); % floes diameter vector size allocation
    Dmax(find(C)) = D;            % floes diameter vector
end
% Waves
fmin  = 1/20;                    % minimum wave frequency
fmax  = 1/2.5;                   % maximum wave frequency
om1   = 2*pi*fmin;               % minimum wave radial frequency
om2   = 2*pi*fmax;               % maximum wave radial fequency
nw    = 61;                      % number of frequency bins
dw    = (om2-om1)/(nw-1);        % integral interval for wave radial frequencies
om    = om1+(0:nw-1)'*dw;        % wave radial frequencies vector
T     = 2*pi./om;                % wave periods vector
Ei    = JONSWAP(Tm,Hs,om);       % JONSWAP spectrum
wlng  = g.*T.^2./(2.*pi);        % wavelength as a function only of wave period
cp    = sqrt(g.*wlng./(2.*pi)); % phase speed
cg    = cp./2;                   % group speed
cgmax = max(cg);                 % group speed maximum
cg(:) = cgmax;                   % no dispersion = all group speed are the same
        (maximum)
% Wind
U10 = repmat(U10,nx,1); % wind speed at 10m elevation vector
% Temporal grid
dt     = dx/cgmax;       % time interval (temporal resolution)
nsteps = nx+1;           % number of time steps (=nx+1 because advection is
                         % done from one cell at each time step)
time   = 0:dt:nsteps*dt; % time vector
nt     = length(time);   % time vector size
% Memory preallocation
E        = zeros(nx,nw); % wave spectrum
Swin     = zeros(nx,nw); % wind source term
Swcp     = zeros(nx,nw); % white-capping source term
Sice     = zeros(nx,nw); % ice dissipation source term
S_win    = zeros(nx,nw); % wind source term weighted by open water fraction (for
         outputs)
S_ice    = zeros(nx,nw); % ice dissipation source terme weighted by ice fraction
S_wcp    = zeros(nx,nw); % white-capping source term weighted by open water
         fraction
Hsig     = zeros(1,nx);  % significant wave height
% Action density limiter
Slim = action_density_limiter(om,cp); % SEE action_density_limiter routine
for n=1:nt     % Time loop
    % Advection.
    % The advection is done by solving Dt(S) = 0 using the
    % Lax-Wendroff scheme with Superbee flux limiting and a Neumann
    % boundary condition. The advection is performed over the whole domain
    % in one step on an unattenuated intermediate spectrum.
```

```
    for w=1:nw % Advection loop over each frequency
        E(:,w)   = advection(E(:,w),cg(w,:),dx,dt); % SEE advection routine
    end
    % Incident wave spectrum
    E(1,:) = Ei; % The initial wave spectrum is forced in the first cell
    % Processes for each spatial cell with ice (generation by wind, dissipation
    % by white-capping and attenuation by ice)
    for i=1:nx % Spatial loop
        % Generation by wind
        Swin(i,:) = wind_gen(U10(i),E(i,:),om,cp); % SEE wind_gen routine
        Swin(i,:) = min(Swin(i,:),Slim');           % action density limiter
        E(i,:) = E(i,:) + Swin(i,:)*dt*(1-cice(i)); % the wave spectrum is updated
         (explicit scheme)
        S_win(i,:) = Swin(i,:)*(1-cice(i));         % effective wind source term
         for outputs
        % Dissipation by white-capping
        Swcp(i,:) = white_cap(E(i,:),om,cp); % SEE white-cap routine
        Swcp(i,:) = max(Swcp(i,:),-Slim');          % action density limiter
        E(i,:) = E(i,:) + Swcp(i,:)*dt*(1-cice(i)); % the wave spectrum is updated
         (semi-implicit scheme)
        S_wcp(i,:) = Swcp(i,:)*(1-cice(i));         % effective white-capping
         source term for outputs
        % Attenuation by ice
        if cice(i)>0
            Sice(i,:) = ice_att(E(i,:),T,cg,cice(i),hice(i),Dmax(i),dt*cice(i)); %
         SEE ice_att routine
            E(i,:) = E(i,:) + Sice(i,:)*dt*cice(i); % the wave spectrum is updated
         (implicit scheme)
        else
            Sice(i,:) = 0;                          % if there is no ice, there is
         no attenuation
        end
        % Wave spectrum statistics
        E(E<0) = 0;                                 % avoiding negative energy
        m0 = trapz(om,E(i,:));                      % total energy
        Hsig(i) = 4*sqrt(m0);                       % significant wave height
    end
end

end
```

```
function E = advection(E,c,dx,dt)
%ADVECTION  is a 1d advection code Lax Wendroff scheme with Superbee flux limiter
%
% INPUTS:
%   E  = vector of the thing to be advected;
%   c  = scalar speed;
%   dx = the spatial resolution;
%   dt = the temporal resolution;
%
% OUTPUT:
%   E  = vector of the thing to be advected - after advection;

if ~isequal(size(E),size(c))
    c = c';
end

f  = flux(E,c,dx,dt);
E  = E-dt*diffl(f)/dx;

function f = flux(E,c,h,dt)
   % Lax-Wendroff with Superbee flux limiting;
   theta = diffl(E)./(diffr(E)+3e-14);
   phi   = limiter(theta);
   f     = c.*E+c/2.*(1-c*dt/h).*diffr(E).*phi;
end


function y = diffl(x)
y = [0;diff(x)];
end

function y = diffr(x)
y = [diff(x);0];
end

 % Superbee
function phi = limiter(r)
    phi = max(0,max(min(1,2*r),min(r,2)));
end
end
```

```
function [S_ice] = ice_att(E,T,cg,cice,h,Dave,dt)
%ICE_ATT calculates the wave attenuation by ice.
%
% INPUTS
% E     = initial wave energy vector
% T     = wave periods vector
% cg    = wave group speeds vector
% cice  = ice concentration
% h     = ice thickness
% Dave  = floe average diameter
% dt    = temporal resolution
%
% OUTPUTS
% S_ice = ice source term

% Polynomial coefficients to reconstruct the attenuation coefficient of
% Kohout and Meylan (2008)
q11 = -0.00000777;
q12 =  0.00032080;
q13 = -0.00437542;
q14 =  0.02047559;
q15 = -0.01356537;
q21 =  0.00003635;
q22 = -0.00153484;
q23 =  0.02121709;
q24 = -0.09289399;
q25 = -0.03693082;
q31 = -0.00004509;
q32 =  0.00214484;
q33 = -0.03663425;
q34 =  0.26065369;
q35 = -0.62474085;
p1 = q11.*T.^4 + q12.*T.^3 + q13.*T.^2 + q14.*T + q15;
p2 = q21.*T.^4 + q22.*T.^3 + q23.*T.^2 + q24.*T + q25;
p3 = q31.*T.^4 + q32.*T.^3 + q33.*T.^2 + q34.*T + q35;
a = @(x,y) p1.*h.^2 + p2.*h + p3;
% Scattering coefficient
if h > 5.0
    alpha = -1*a(T,5.0);
elseif h < 0.4
    alpha = -1*a(T,0.4);
else
    alpha = -1*a(T,h);
end
alpha = alpha';
alpha(alpha<0) = 0;
% Attenuation
att = alpha*cice/Dave.*cg'*dt;
if dt>0
    S_ice = (exp(-att)-1).*E/dt;
else
    S_ice = 0;
end
end
```

```
function [S] = wind_gen(U10,E,om,c)
%WIND_GEN computes the wind input source term
%
% INPUTS
%   U10 = wind speed at 10m elevation. U10 is a scalar.
%   E   = wave spectrum in m²/Hz.
%   om  = radial frequency range.
%   c   = phase speed.
%
% OUTPUTS
%   S   = wind input source term.

rho_air = 1;    % air density
rho_wtr = 1025; % water density
g       = 9.81; % gravitational acceleration
% drag coefficient
if U10 < 7.5
    CD = 1.2875e-3;
else
    CD = (0.8 + 0.065*U10)*10e-3;
end
u_str  = sqrt(CD*U10^2);                                % wind friction velocity
w_PM   = 2*pi*0.13*g/(28*u_str);                        % Pierson-Moscowitz
         frequency
G      = exp(-(om/w_PM).^-4);                           % cut-off fonction to avoid
         irrealistic growth for short waves
a      = (1.5e-3*u_str^4*G)/(g^2*2*pi);                 % linear growth term
a      = 0;                                             % a = 0 when waves
         initially exist
b      = om.*0.25*rho_air/rho_wtr.*(28*(u_str./c)-1); % exponential growth term
b(b<0) = 0;                                             % avoiding negative values,
         so that the waves cannot transfer energy to the air
S      = a' + b'.*E;                                    % wind input source term

end
```

```
function [S_wc] = white_cap(E,om,cp)
%WHITE_CAP compute the white-capping source term.
%
% INPUTS
%   E  = wave spectrum in m²/Hz.
%   om = radial frequency range
%   cp = phase speed.
%
% OUTPUTS
%   S_wc = white-capping source term.

if E == 0
    S_wc = 0;
    return
else
    m0   = trapz(om,E);                                % 0th order moment (total
        energy)
    wm   = ((1/m0)*trapz(om,E./om'))^-1;               % mean frequency
    km   = ((1/m0)*trapz(om,E.*sqrt((cp./om))'))^-2; % mean wavenumber
    sm   = km*sqrt(m0);                                % overall steepness
    sPM  = sqrt(3.02e-3);                              % Pierson-Moscowitz overall
        steepness
    Cwc  = 2.36e-5;                                    % coefficient
    p    = 4;                                          % coefficient
    mu   = Cwc*(sm/sPM)^p*(wm/km);
    S_wc = -mu*(om./cp)'.*E;                           % white-capping source term
end

end
```

```
function [N] = action_density_limiter(om,cp)
%ACTION_DENSITY_LIMITER compute the maximum spectral evolution of waves
%
% INPUTS
%   om = radial frequency range
%   cp = phase speed
%
% OUTPUTS
%   N = maximum every source term can reach

k = om./cp; % wavenumber
cg = cp./2; % group speed
gam = 0.1;  % factor
alPM = 8.1e-3; % Pierson-Moscowitz cut-off frequency
N = gam*alPM./(2*om.*k.^3.*cg);

end
```